Highly Transmission Efficiency of Optoelectronic Devices Using Active Hybrid Plasmonic Coupler

samar elsayed elbialy (samarelbialy03@gmail.com)
Delta University https://orcid.org/0000-0001-5708-8021
Bedir Yousif
Mansoura University
Ahmed Samra
Mansoura University

Research Article

Keywords: Plasmonics, Bidirectional Coupler, MOS Waveguides, Photonic integrated circuits, SOI waveguides

Posted Date: March 11th, 2021

DOI: https://doi.org/10.21203/rs.3.rs-256240/v1

Highly Transmission Efficiency of Optoelectronic Devices Using Active Hybrid Plasmonic Coupler

Samar Elbialy[1]. Bedir Yousif[2,3]. Ahmed Samra[4]

Corresponding author:

Samar Elbialy[1]
Email address: samarelbialy03@gmail.com
Telephone numbers: +20 01011109369
1- Communications and Computer Department, Faculty of Engineering, Delta University for Science and Technology, Gamasa, Egypt.

Secondary authors:

Bedir Yousif[2,3]
Email address: bedir.yousif@gmail.com
Telephone numbers: +20 01062602180
2- Electrical Engineering Department, Faculty of Engineering, Kafrelsheikh University, Kafrelsheikh, Egypt.
3- Electrical Engineering Department, Faculty of Engineering and information technology, Onaizah Colleges, Al-Qassim, KSA.

Ahmed Samra[4]
Email address: ahsamra@yahoo.co.uk
Telephone numbers: +20 01224053523
4- Electronics and Communications Department, Faculty of Engineering, Mansoura University, Mansoura, Egypt.

Abstract

This paper discusses modeling and optimizing the performance of hybrid plasmonic bidirectional coupler which is used as a basic building block in modeling highly transmission efficiency of optoelectronic devices such as filter, wavelength division multiplexer, logic gates and switching matrix with a help of an active material (indium tin oxide) that has an electrically-adjustable permittivity. All the proposed devices satisfied high transmission efficiencies at the desired output ports over a suitable wavelength range. The realized structures are characterized and simulated by 3D finite-difference time-domain (FDTD). The components would be useful in the optical interconnect networks, photonic integrated circuits and signal processing system.

Keywords: Plasmonics; Bidirectional Coupler; MOS Waveguides; Photonic integrated circuits; SOI waveguides.

1. Introduction

Designing and improving the performance of Nano- optical plasmonic devices has acquired a major saucepan of interest over the last decade, because of the expansion of numerical modeling techniques and the progress in production technologies [1]. During this, signal transmutation faces some defects which were recently overcome by interbreeding plasmonics with semiconductors, dielectrics and photonics [2-3], and this achieves many advantages such as sturdy mode retention and reducing the propagation loss [4-5].

Designing of Nano-optical plasmonic devices by using the Electro-Optic technique has been used to satisfy active control in the signal' modulation directions [6-9]. Based on the compatibility between the silicon-on-insulator (SOI) waveguides and the complementary metal-oxide-semiconductor (CMOS) fabrication processes, a cost-efficient mass production milieu for integrated photonic devices can be guaranteed [10-11].

This work proposes a signal modification whose active mechanism Attributed to the Electro-optic technique and this has been implemented using hybrid plasmonic waveguides. The signal' modulation mechanism is satisfied by varying the refractive index of the active medium, a thin layer inside the MOS waveguide, via applying an external voltage on the MOS waveguide and this leads the effective index of the optical mode to be shifted and hence the modal overlap between the neighboring waveguides has been changed [12-13]. The active material which are merged between the layers of MOS waveguide is called indium tin oxide (ITO) which belongs to the family of transparent conductive oxides (TCOs) [14].

Transparent conductive oxides are oxide' semiconductors that have been utilized in optoelectronic structures because of their strong nonlinear response, electrically-tunable permittivity, and fast energy transfer [15-16]. Indium tin oxide (ITO) was chosen for this task due to its unity-strong index tenability. Its modulation mechanism depends on alternating the free carrier concentration that forces the plasma frequency of the dispersion relation to be shifted [17-18].

The proposed structures have been simulated via the three-dimensions finite-difference time-domain (3D-FDTD) solver which depended on the perfectly matched layer (PML) in terminating the simulation domain [19].

2. Background

The Material Database used in the simulation tools stores the material data (permittivity) obtained from the handbook of "Optical Constants of Solids I – III" by "E. Palik". Palik's handbook of optical constants is one of the most cited references for a number of common materials including the materials used in this research such as silicon dioxide (SiO_2), silicon (Si), and noble metals such as gold (Au) and silver (Ag) [20].

The Drude model characterizes the noble metals' conductivity over a wide range of wavelengths, in which, the metal's conductivity can be transformed to permittivity. In Drude model, the metal's dielectric constant is defined as [21]:

$$\varepsilon(\omega) = \varepsilon_{\infty} - \frac{{\omega_p}^2}{\omega(\omega + i\Gamma)} \quad (1)$$

Where; ($\varepsilon_{\infty} = 3.7$) is the dielectric constant at infinite angular frequency, ($\omega_P = 1.38 * 10\text{^}16$ Hz) is the plasma frequency of free conduction electrons' oscillations of, ($\Gamma = 2.73 * 10\text{^}13\ Hz$) is the damping frequency and ($f = \omega/2\pi$) is the frequency of incident wave.

The Drude model can provide good estimation for the dielectric constants of metals at wavelengths longer than the visible and the near-IR wavelength range. The wavelength range used in this thesis is (1300-1800) nm, so the Drude model can be very accurate for our study.

The present work is structured as follows; section (3) proposes Modeling of Hybrid Plasmonic Bidirectional Coupler, this design is reused as a 2x2 Electro-Optic Switch and NOT Logic Gate as illustrated in section (4). Section (5) proposes the bidirectional plasmonic coupler as a base unit for building more advanced structures such as filter which reused again as a 3x3 switching matrix and a wavelength division multiplexer. Section (6) and section (7) propose modeling of a 5x5 switching matrix and different logic gates, respectively.

3. Modeling of Hybrid Plasmonic Bidirectional Coupler

Modeling and performance enhancement of hybrid plasmonic bidirectional coupler is necessary to support the development of Nano-optical communication systems.

The proposed hybrid plasmonic bidirectional coupler consists of two units; a) the base unit, which consists of two SOI strip waveguides; b) the control unit is MOS multilayer-slab waveguide.

The base unit for the realized hybrid plasmonic bidirectional coupler consists of a two core SOI waveguide which illustrated in figure (1). The silicon-on-insulator (SOI) waveguides have been considered an important component in photonic integrated circuits (PICs), as directional couplers, because it has proven its efficiency in the applications of high-speed CMOS chips. The SOI waveguide consists of a Si-ridge printed on a substrate of SiO_2, the high confinement of electromagnetic field into the silicon core is considered the major advantage of this waveguide.

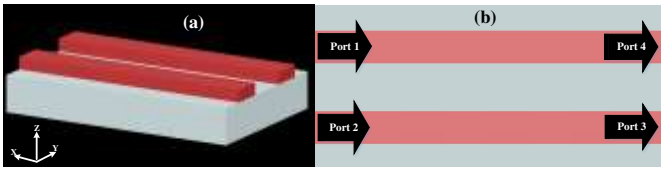

Figure 1: the schematic of base unit (two SOI strip waveguides); a) 3D- view, and b) 2D- XY view.

The structure is targeted to operate at the telecommunication wavelength ($\lambda = 1550\ nm$), where silicon is transparent. According to the simulation method, the electric field intensity distribution over the design in the XY plane at the middle of Si layer is chosen to prove the good confinement function in the silicon core as shown in figure (2). In order to achieve the switching mechanism, a control unit must be used.

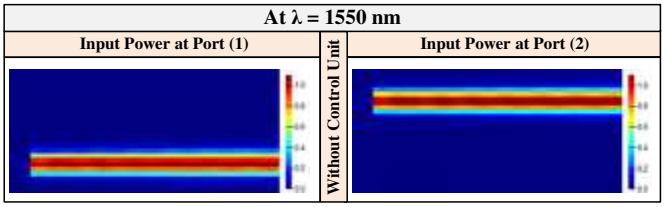

Figure 2: the distribution of electric field (E) intensity for the base unit (two SOI strip waveguides) without control unit.

The control unit is a hybrid plasmonic multilayer waveguide centered between the two SOI waveguides which illustrated in figure (3). The hybridization technique satisfies strong mode confinement and reduces the propagation loss.

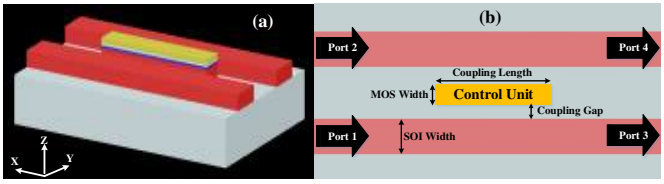

Figure 3: the schematic of the proposed bidirectional coupler after adding the control unit; a) 3D- view, and b) 2D- XY view.

The coupling function mainly depends on the control unit which is a metal-oxide-semiconductor (MOS) waveguide which achieves the hybridization between a noble metal (silver), oxide material (SiO_2) and semiconductor material (Si). A thin layer of an active material is added between the MOS' waveguide layers, whose optical properties changes from dielectric to a quasi-metal according to a biasing voltage which is applied to the MOS waveguide as illustrated in figure (4).

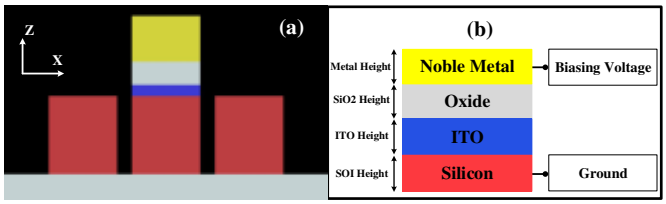

Figure 4: a) the 2D- XZ view of bidirectional coupler, and b) the construction of MOS waveguide.

The selected active material in this work is indium tin oxide (ITO) because of its unity-strong index tenability, its modulation mechanism is to change the free carrier concentration of the material overlapping with the propagating optical mode which leads to a shift of the plasma frequency of the dispersion relation [17-18]. This modifies both the real and imaginary parts of the refractive index of the material, and henceforth alters the index and loss of the optical propagating mode.

The MOS waveguide is forward biased, i.e. a high voltage at the noble metal-layer and a low voltage at the Si-layer. This forming an accumulation layer at the ITO-oxide interface which can change the super optical mode' index.

The structure is tested at the telecommunication wavelength ($\lambda = 1550\ nm$) by using the simulation tools, as shown in figure (5). the electric field intensity distribution over the design in the XY plane prove the coupling function after adding the control unit.

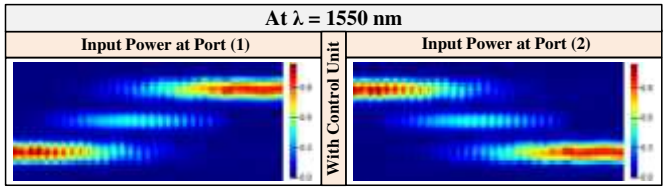

Figure 5: the distribution of electric field (E) intensity for the proposed bidirectional coupler after adding the control unit.

Based on the previous experimentally-proven averaged data for indium tin oxide (ITO) material in [22-25], it is noticeable that the index change of the material depends on its thickness as well as the biasing voltage. A summary for a group of ITO properties at forward biasing listed in table (1).

Table 1: A summary for group of ITO properties.

Thickness = 10 nm [22]				Thickness = 8 nm [23]			
Bias = 0 volt		Bias = 4 volt		Bias = 0 volt		Bias = 12 volt	
n	k	n	k	n	k	n	k
1.946	0.002	1.042	0.273	-1.67	0.825	-1.95	0.867
Thickness = 20 nm [24]				Thickness = 8 nm [25]			
Bias = 0 volt		Bias = 4 volt		Bias = 0 volt		Bias = 10 volt	
n	k	n	k	n	k	n	k
1.96	0.002	0.471	0.643	-1.667	0.824	-1.721	0.832

3.1. The Operation of Hybrid Plasmonic bidirectional coupler

According to table (1), the properties of active material (ITO) were chosen as following: thickness of ITO layer = 20 nm, the biasing voltage changes from zero volt (OFF state) to 4 volts (ON state) and hence the refractive index of ITO changes from 1.96+i0.002 to 0.471+i0.643, respectively. According to the previous research [24], these properties are considered to be the best during manufacturing. There are two cases for transferring power from input port to output ports as listed in table (2).

Table 2: the two cases for transferring power during the bidirectional coupler.

Input power at port (1)		Input power at port (2)	
The input power is totally transferred to the next waveguide	The input power remains on its path	The input power remains on its path	The input power is totally transferred to the next waveguide
Output power		Output power	
port (4)	port (3)	port (4)	port (3)
The control unit' state		The control unit' state	
CROSS state	BAR state	BAR state	CROSS state
The biasing voltage		The biasing voltage	
Sit to zero volt (OFF state)	Sit to 4 volts (ON state)	Sit to 4 volts (ON state)	Sit to zero volt (OFF state)

The performance of the bidirectional coupler is affected by the dimensions chosen during its design. These dimensions are as follows: a) the coupling length of the device, b) the dimensions of two SOI strip waveguides, c) the dimensions of MOS multilayer slab waveguide, and d) the coupling gap between the three waveguides.

First, the optimum coupling length of the device, where the control unit sit to CROSS state, can be determined using equation (1) as in [22]

$$L_c = \left(\frac{\lambda}{2\Delta N_{eff}}\right) \quad (2)$$

Where λ the free space light operating wavelength, and ΔN_{eff} is the effective mode index difference between the first two symmetric transverse magnetic (TM) modes within the MOS waveguide. And then the third effective TM mode index is used to calculate the optimized oxide height, the layer in MOS waveguide, by the matching equation (3) as in [22]:

$$2N_{eff_{TM_3}} = \left(N_{eff_{TM_1}} + N_{eff_{TM_2}}\right) \quad (3)$$

From another point of view, it is suggested that the coupling length of routing switch can be equal to an integer of the desired coupled mode wavelength $(n\lambda)$ [24].

After studying the effect of changing the dimensions of the coupling gap and the width of MOS waveguide on the performance of the device, we find that the efficiency of the device is negatively affected with the increase in the width of the coupling gap as well as the width of the MOS waveguide, and this leads to an increase in coupling length (becomes longer), that is, an increase in the size of the device in order to improve the efficiency again. This was demonstrated by the analyzed results shown in figure (6).

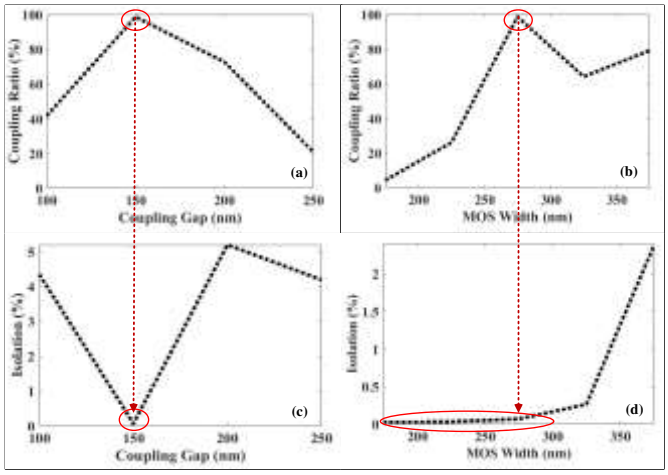

Figure 6: the analyzed results of coupling ratio (CR) as a function of a) the gap width and b) the MOS waveguide width at the optical communication wavelength (1550 nm).

The aim of the optimization process is to achieve the highest efficiency ratio (increase the coupling ratio and reduce the isolation ratio) and at the same time reduce the dimensions of the device. After reaching the optimized value of both the Coupling Length and the Oxide Height, by achieving equations 1 and 2, the next step is to calculate the optimized value of both MOS Width and Coupling Gap. The performance of the device is tested after using the optimized values for each of the Coupling Length which is $\approx (5\lambda)$ and the Oxide Height which is 20 nm taking into account the change of the MOS Width and Coupling Gap values as shown in figure (6).

As can be seen through figure (6-a) and (6-c), we find that when the Coupling Gap equals to 150 nm, the highest coupling ratio and the lowest isolation ratio are achieved. So, we consider the optimized Coupling Gap to be 150 nm. After using the optimized Coupling Gap in addition to the above we find that when the MOS Width equals to 275 nm, the highest coupling ratio and the lowest isolation ratio are achieved as shown through figure (6-b) and (6-d).

3.2. The Characteristics of Hybrid Plasmonic Bidirectional Coupler

After implementing the optimization scenario and obtaining the desirable parameters or optimized parameters used in the design of the device, this device is used as a bidirectional coupler, whose schematic is shown in figure (7), and the parameters used in the design are listed in table (3).

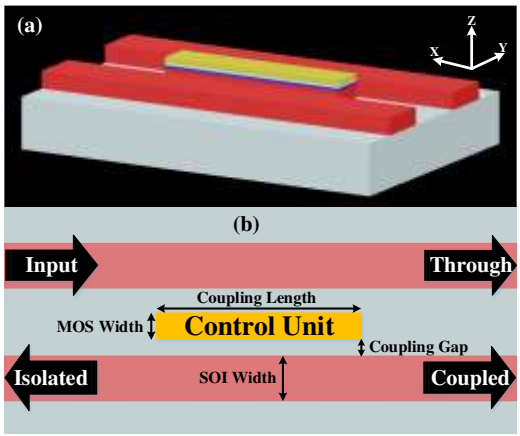

Figure 7: a) 3D- view, and b) 2D- XY view of hybrid plasmonic 2x2 bidirectional coupler.

Table (3): the design parameters of hybrid plasmonic bidirectional coupler

The biasing voltage			
zero volt		4 volts	
ITO' refractive index	1.96+i0.002	ITO' refractive index	0.471+i0.643
Control Unit	CROSS state	Control Unit	BAR state
The thickness of ITO layer		20 nm	
Coupling length		8 µm	
Oxide height		20 nm	
Metal height		100 nm	
MOS width		275 nm	
Coupling gap		150 nm	
SOI dimensions of through and coupled waveguides		400 nm x 340 nm	
SOI dimensions of MOS waveguide		275 nm x 340 nm	

The coupling process depends fundamentally on the properties of active layer. After exciting the proposed bidirectional coupler with an optical mode of a polarized transverse magnetic (TM) type which injected into the input port, two states of transferring power are appeared: a) when the control unit becomes BAR, the output power appeared at the Through port, b) when the control unit becomes CROSS, the output power appeared at the Coupled port.

The performance of hybrid plasmonic bidirectional coupler can be analyzed by using the following parameters [22-23]:

a) Coupling Ratio (CR)

$$CR_{Through}\ (\%) = 100 * \left(\frac{Power_{Through}}{Power_{Through} + Power_{Coupled}}\right) \quad (4.1)$$

$$CR_{Coupled}\ (\%) = 100 * \left(\frac{Power_{Coupled}}{Power_{Through} + Power_{Coupled}}\right) \quad (4.2)$$

b) Isolation

$$Isolation_{Through}\ (\%) = 100 * \left(\frac{Power_{Through}}{Power_{Isolated}}\right) \quad (5.1)$$

$$Isolation_{Coupled}\ (\%) = 100 * \left(\frac{Power_{Coupled}}{Power_{Isolated}}\right) \quad (5.2)$$

3.3. The Performance of the Hybrid Plasmonic Bidirectional Coupler

A more compact and efficient hybrid plasmonic coupler is produced in this work by using the design parameters listed in table (3) in the device' fabrication.

The performance of the optimized hybrid plasmonic bidirectional coupler can be tested by using simulation tools known as Lumerical 3D-FDTD Solutions, and after placing power monitors at the input/output ports, the device performance can be tested via those factors listed in equations (4 and 5).

The device coupling mechanism is satisfied by varying the index of the optical mode according to the biasing voltage of the external control signal, as mentioned in section (3.1).

The execution of the simulated bidirectional coupler is experimented through a suitable range of wavelengths (1500-1600) nm. The analyzed results of coupling ratio (CR), and isolation through this chosen range are illustrated at figure (8).

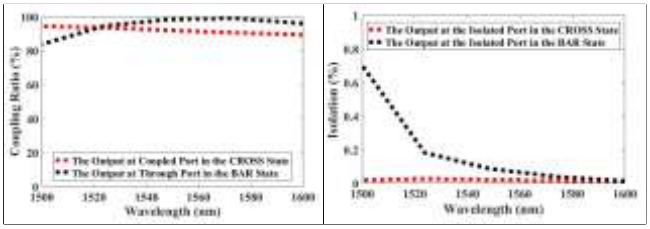

Figure 8: the analyzed results of coupling ratio (CR) and isolation as a function of wavelength.

According to figure (8), the CR values that obtained in the two cases of the bidirectional coupler (Through and Coupled) are greater than 80% at the desired output port; also, the obtained insertion ratio values are less than 0.8%.

The electric field intensity distribution through the bidirectional coupler in the XY plane at telecommunication wavelength is shown in figure (9) which illustrates the coupler functionality.

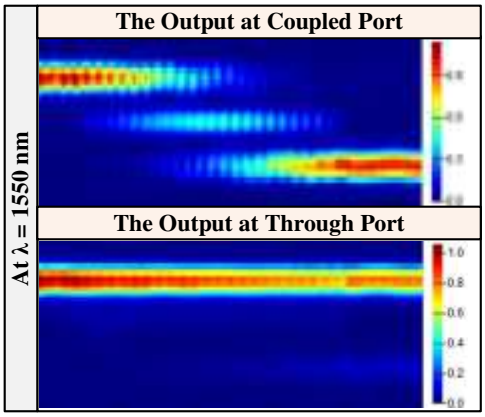

Figure 9: the distribution of electric field (E) intensity at Coupled / Through states of the proposed bidirectional coupler.

To complete the optimization process, two different metals, namely gold and silver, were used to test the performance of the device and achieve the highest efficiency. After analyzing the results that we obtained, which are represented in coupling ratio and isolation values, it became clear that these results are close to some extent.

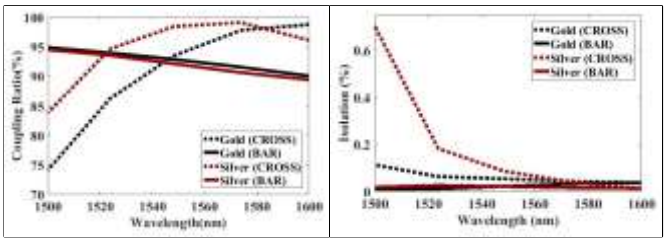

Figure 10: a comparison between the coupler's performance in terms of coupling ratio and isolation in the case of using gold and silver as noble metals over a specified range of wavelengths.

For example, at the telecommunication wavelength, we find that when using silver as a metal electrode, this satisfies a coupling ratio of 98.488 % and an isolation value of $8.74*10^{-2}$ % at CROSS state. And on the other hand, when using gold as a metal electrode, this achieves a coupling ratio of 93.55 % and an isolation of its amount $5.48*10^{-2}$ %. Accordingly, the silver was chosen to be the metal electrode used during the design of the plasmonic bidirectional coupler. The proposed results are utilized to make a validation with the results obtained in reference [24], as illustrated in table (4).

Table 4: a comparison between the performance of two different bidirectional coupler.

Parameter		Present work	Reference [24]
Coupling length (μm)		8	30
Active Layer		ITO	GST
Wavelength range (nm)		(1500 - 1600)	(1520 - 1550)
Transmission	Desired	(80 - 100) %	(60 - 80) %
	Undesired	(0.8 - 15) %	(0.5 - 3) %

4. Using Hybrid Plasmonic Bidirectional Coupler as a Multi-functional Device

The new trend in technology aspires to design a multi-functional device, that uses this to skip the large-scale photonic integrated circuits and the system' complexity problems, so the bidirectional coupler explained in the previous section will be re-used in various ways to support modeling of Nano-optical plasmonic devices for communication systems.

4.1. Using Hybrid Plasmonic Bidirectional Coupler as a 2x2 Electro-Optic Switch

The same schematic used for bidirectional coupler that proposed in section (3) with the same design' parameters in terms of dimensions and materials will be used to display the performance of the device again, but in the form of a 2x2 Electro-Optic Switch as illustrated in figure (11).

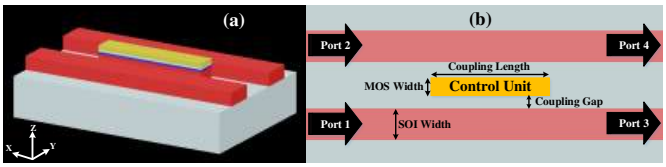

Figure 11: a) 3D- view, and b) 2D- XY view of hybrid plasmonic 2x2 electro-optic switch.

Assuming that the input power is injected into port (1), we find that it travels in two different ways depending on the state of the control unit. If the control unit is in its CROSS' state, then the input power is transferred to the adjacent waveguide and the output power appears on port (4), while if the control unit is in its BAR state the power stays in the same waveguide and the output power appears on port (3).

The switch performance can be tested via a group of factors as following [24-25]:

1) Insertion loss

$$IL_{Port\,(3)}(dB) = 10 * Log\left(\frac{Power_{Port\,(3)}}{Power_{Port\,(1)}}\right), \qquad (6.a)$$

if control unit is in its BAR state

$$IL_{Port\,(4)}(dB) = 10 * Log\left(\frac{Power_{Port\,(4)}}{Power_{Port\,(1)}}\right), \qquad (6.b)$$

if control unit is in its CROSS state

2) Extinction ratio

$$ER_{Port\,(3)}(dB) = 10 * Log\left(\frac{Power_{Port\,(3)}\ at\ BAR\ state}{Power_{Port\,(3)}\ at\ CROSS\ state}\right) \qquad (7.a)$$

$$ER_{Port\,(4)}(dB) = 10 * Log\left(\frac{Power_{Port\,(4)}\ at\ CROSS\ state}{Power_{Port\,(4)}\ at\ BAR\ state}\right) \qquad (7.b)$$

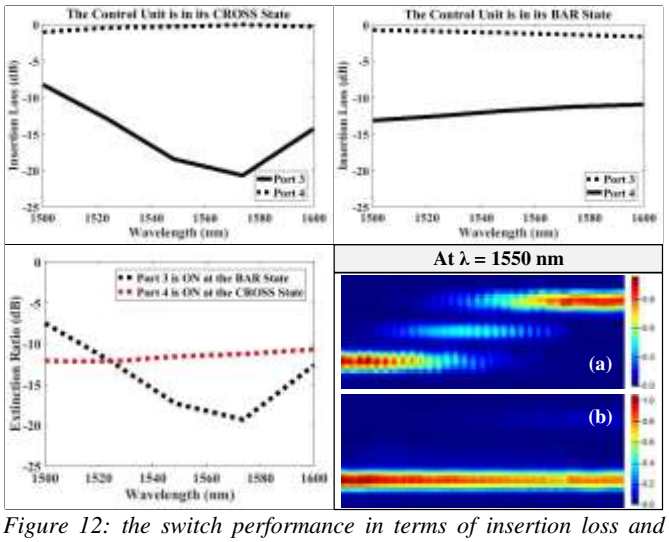

Figure 12: the switch performance in terms of insertion loss and extinction ratio at the two states of control unit. the distribution of electric field (E) intensity at a) CROSS state and b) BAR state over the switch in the XY plane.

Based on the simulation results that have been obtained from Lumerical 3D-FDTD Solutions, the switch performance can be tested via those factors explained in equations (6, and 7). The analyzed results of extinction ratio (ER) and insertion loss (IR) over the selected wavelength range are shown at figure (12). In addition, the electric field intensity distribution over the routing switch in the XY plane at telecommunication wavelength (1550 nm) is used to illustrate the switching mechanism for the proposed device.

4.2. Using Hybrid Plasmonic Bidirectional Coupler as a NOT Logic Gate

plasmonic logic gates are an essential and required components for signal processing in optical communication systems. Recently, many plasmonic structures have been used to implement logic gates as each of them displays the gate with designs, materials, dimensions, frequency range, as well as different transmission efficiencies.

What distinguishes this work is the presentation of the logic gate in a wavelength range as well as appropriate transmission efficiency and at the same time reuse of the bidirectional coupler that was presented in section (3) as a NOT gate, which achieves multi-functional device technology, which is our primary goal here.

The same schematic used for bidirectional coupler that proposed in section (3) with the same design' parameters in terms of dimensions and materials will be used to display the performance of the NOT logic gate, but after deactivate two ports {port (1) and port (4)} as illustrated in figure (13).

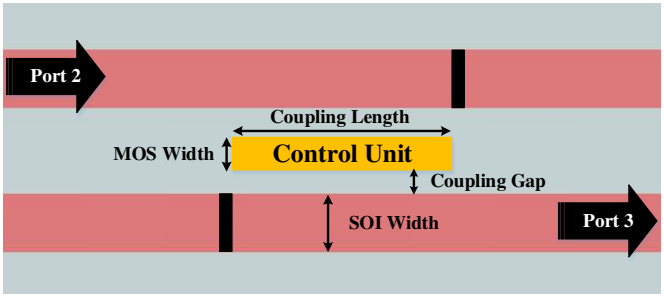

Figure 13: the 2D- XY view of hybrid plasmonic NOT logic gate.

The symbol and the truth table of NOT logic gate is illustrated in figure (14). As is evident from the figure, there are two inputs to the gate, one of which represents the control signal, while the other represents the main input of the gate. As can be seen from the figure, the logic operation of the gate depends mainly on the control signal, taking into account that the input signal is always present.

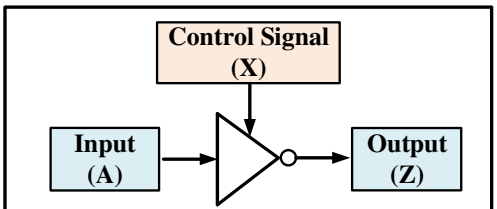

The truth table of NOT gate

A	X	Z
ON	ON	OFF
ON	OFF	ON

Figure 14: the symbol and the truth table of hybrid plasmonic NOT logic gate.

Figure (15) shows the performance of the logic gate by using the transmission value, which is calculated from equation (8)

$$\boldsymbol{Transmission}\ (\%) = \mathbf{100} * \left(\frac{\boldsymbol{Power}_{Port\,(3)}}{\boldsymbol{Power}_{Port\,(2)}}\right) \qquad (\mathbf{8})$$

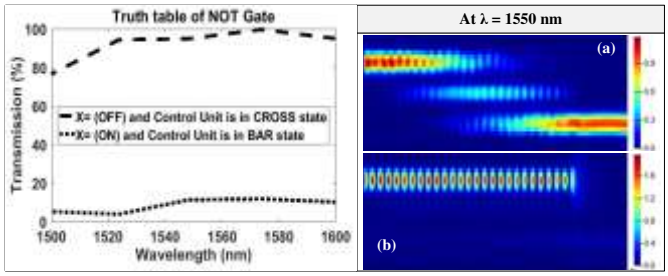

Figure 15: the NOT gate performance in terms of transmission as a function of wavelength, and the distribution of electric field (E) intensity at the two states of truth table over the switch in the XY plane a) X=OFF and Z=ON, b) X=ON and Z=OFF.

When the control signal is on the 4-volt mode, or in other words, the control unit is in the BAR state, this means that the input represents the Logic 1 and it is output in this case is Logic 0. While when the control signal is in the 0-volt mode, or in other words, the control unit is in the CROSS state, this means that the income represents Logic 0, and the output in this case is Logic 1.

5. Modeling of Hybrid Plasmonic Filter

The proposed design of bidirectional plasmonic coupler discussed in section (3) with the same design' parameters in terms of dimensions and materials is considered a base unit for building more advanced structure subject to the use of the same materials. The design developed from the coupler is filter which is considered one of the most important components used in optical communication systems. A suggested schematic design for the filter is shown in figure (16). Taking into consideration that the input ports (1, and 3) are not activated.

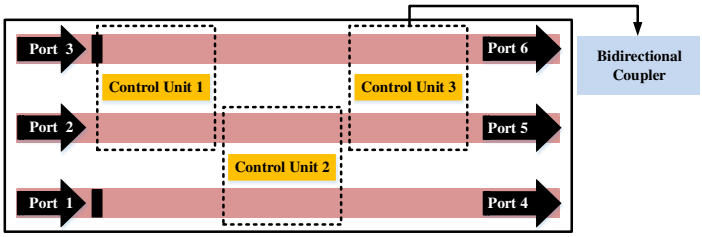

Figure 16: the 2D- XY view of hybrid plasmonic filter.

The input optical power is injected through port (2) while the output appears on the ports (4, 5, and 6). This structure can model different types of filters (Low Pass Filter, Band Reject Filter, and Band Pass Filter) depending on the state of the control units used. Table (4) shows the different types of filters modeled according to the state of the control units.

Table 4: the filter' type according to the state of the control units.

Filter' type	Control Unit 1	Control Unit 2	Control Unit 3
LPF	BAR	BAR	BAR
BRF	BAR	CROSS	BAR
BPF	CROSS	CROSS	CROSS

The structure proposed in figure (16) can be tested by using the Lumerical 3D-FDTD Solutions tools where the device is excited with a transverse magnetic (TM) polarized light at the input port (2) in X- direction (propagation direction). After placing power monitors at the input/output ports, the device performance can be tested via equation (9).

$$\boldsymbol{Transmission}_{4,5,and\,6}\,(\%) = \mathbf{100} * \left(\frac{\boldsymbol{Power}_{Port\,(4,5,and\,6)}}{\boldsymbol{Power}_{Port\,(2)}}\right) \qquad (9)$$

The device performance is tested over the wavelength range of (1300-1800). Figures (17, 18 and 19) show the analyzed results of transmission percentage over the selected wavelength range to verify the filtering' function according to the operation mentioned in table (4).

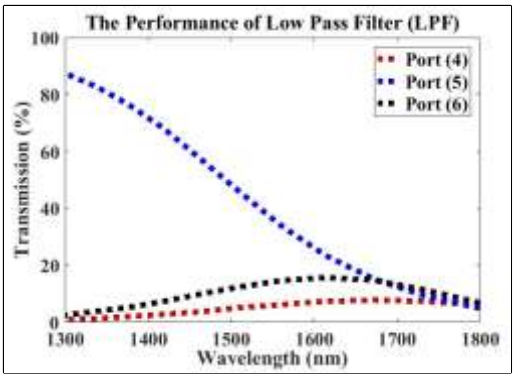

Figure 17: the LPF' performance in terms of transmission as a function of wavelength.

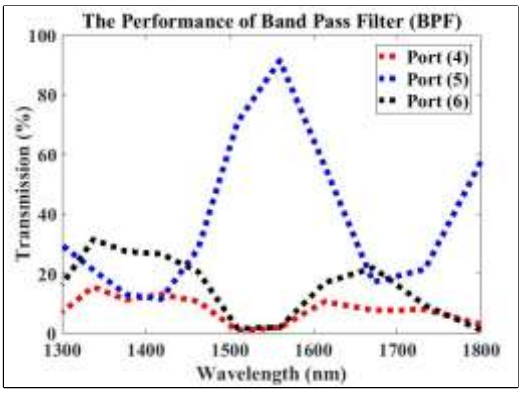

Figure 18: the BPF' performance in terms of transmission as a function of wavelength.

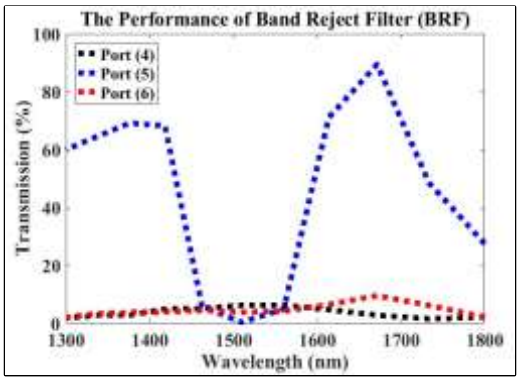

Figure 19: the BRF' performance in terms of transmission as a function of wavelength.

The target wavelength range during the filter performance test is from 1490 nm to 1620 nm, and this band represents the third optical window which is centered at 1550 nm. As is evident from the figures (17, 18, and 19), the filtering' function of the proposed device is proven in the previous specified wavelength range.

5.1. Using the Hybrid Plasmonic Filter as a 3x3 Switching Matrix

To complement the goal to be achieved in this work, which is multi-use device modeling, the hybrid plasmonic filter explained in the previous section will be re-used to support modeling of hybrid plasmonic routing switch which is considered a necessary component for optical communication systems.

The same schematic used for hybrid plasmonic filter that proposed in section (5) with the same design' parameters in terms of dimensions and materials will be used to display the performance of the 3x3 switching matrix, but after activating the two ports {port (1) and port (3)} as illustrated in figure (20).

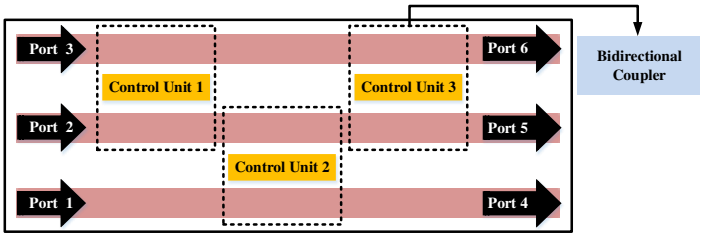

Figure 20: the 2D- XY view of hybrid plasmonic 3x3 switching matrix.

The goal of the switching matrix is to increase the number of input and output ports through which the optical power is transferred in order to serve a greater number of users, and as shown in the figure, the optical power can be injected into any input port {port (1), port (2), or port (3)} and it can also exit from any output port {port (3), port (4), or port (5)}, depending on the state of the control units.

To test the performance of the switch and prove its routing function, random cases will be chosen in which to review the process of transferring the optical power from input ports to output ports.

For example, transferring the optical power from input port (1) to output port (6) needs all the control units to be in its CROSS state. Another example, transferring the optical power from input port (2) to output port (5) needs all the control units to be in its BAR state. The last example, transferring the optical power from input port (2) to output port (4) needs the control units to be as follows; control unit (1) is in its CROSS state, and control units (2, and 3) are in their BAR state.

The 3x3 switching matrix can be tested by using the Lumerical 3D-FDTD Solutions tools where the device is excited with a transverse magnetic (TM) polarized light at the desired input port in X- direction (propagation direction). After placing power monitors at the input/output ports, the device performance can be tested via equation (10).

$$Transmission_{mn}\,(\%) \;=\; 100 * \left(\frac{Power_{Output\ Port\ (n)}}{Power_{Input\ port\ (m)}}\right) \qquad (10)$$

Where m (no. of input port) and n (no. of output port) are integer numbers graded as follows: m = (1,2, and 3) and n = (4,5, and 6). For example, when the optical power transferred from input port (1) to output port (4), we calculate the value of $Transmission_{14}\,(\%)$.

Figure (21) and figure (22) show the analyzed results of transmission percentage over the selected wavelength range and the electric field intensity distribution over the structure in the XY plane at the telecommunication wavelength, respectively. $\{Transmission_{16,\ 24,\ 34,\ and\ 15}\,(\%)\}$ are the randomly selected transmission values for testing the routing' function.

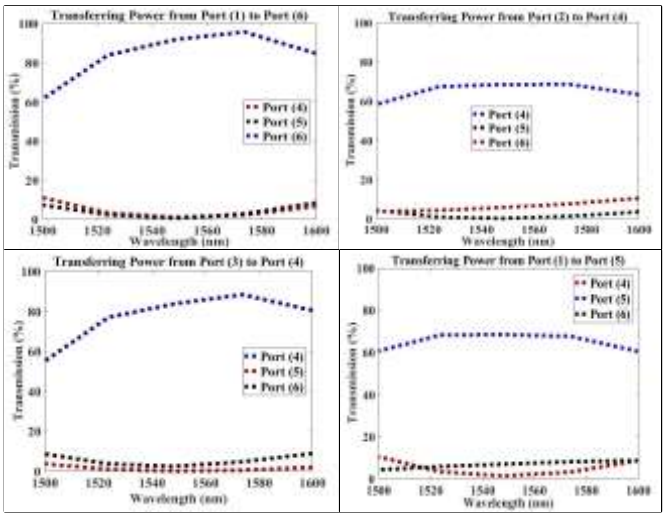

Figure 21: the 3x3 switching matrix' performance in terms of transmission as a function of wavelength.

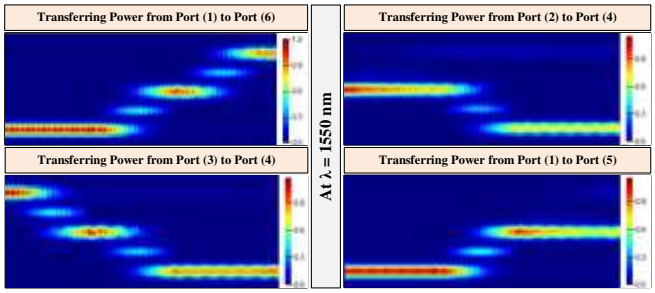

Figure 22: the electric field intensity distribution for 3x3 switching matrix' performance at the telecommunication wavelength.

5.2. Using the Hybrid Plasmonic Filter as a Wavelength Division Multiplexer

To keep up with the growing request of large bandwidth, the transmission capacity has to be increased further. Multiplexing techniques have been proposed as auspicious solutions for satisfying the increasing requests of bandwidth and capacity extension. There are different types of multiplexing techniques such as wavelength division multiplexing, polarization division multiplexing, and time division multiplexing.

The wavelength division multiplexing technology is used to carry information through channels depending on multiple laser light source. The wavelength division multiplexer (WDM) is a major and important component in modernistic optical communication systems. This section presents the principles of realizing the two algorithms for wavelength division multiplexing technology that shown in figure (23).

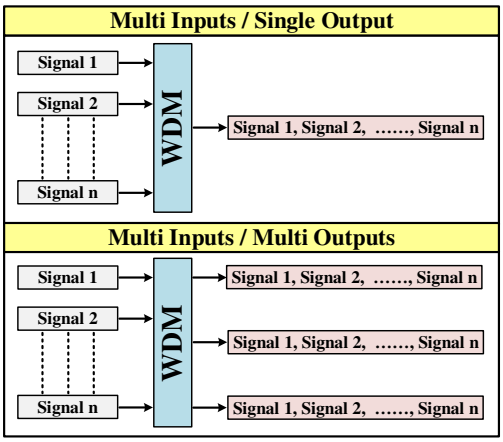

Figure 23: two different algorithms for wavelength division multiplexing technology.

5.2.1. Multi-Inputs / Single-Output Wavelength Division Multiplexer

The same schematic used for hybrid plasmonic filter that proposed in section (5) with the same design' parameters in terms of dimensions and materials will be used to display the performance of three-inputs / single-output WDM, but after deactivating the two output ports {port (4) and port (6)} as illustrated in figure (24).

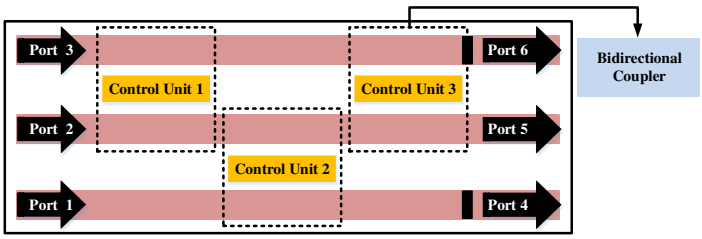

Figure 24: the 2D- XY view of the three-inputs/single-output wavelength division multiplexer.

A polarized light wave of transverse magnetic type is injected at the input ports where each input port carried single wavelength. A wavelength of 1500 nm is injected to Port (1), a wavelength of 1550 nm is injected to Port (2), and a wavelength of 1600 nm is injected to Port (3). Taking into account that all control units appeared in the structure (Control Unit 1, Control Unit 2, and Control Unit 3) are considered in its CROSS state.

According to figure (25), The obtained transmission efficiency values at the selected wavelength range indicate that this structure does not support the usual multiplexing process (the output port carries only the individual wavelengths (1500, 1550, and 1600) nm that injected into the input ports) but the device shows the full wavelength range (1500-1600) nm at the output port.

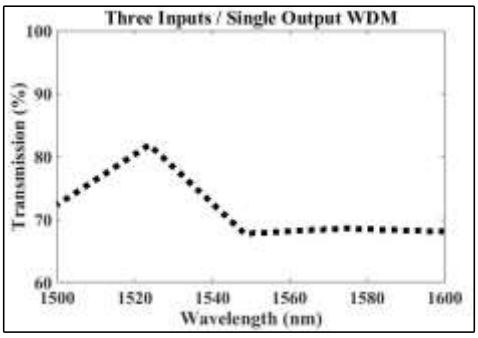

Figure 25: the device' spectrum when input is launched into port (1).

5.2.2. Multi-Inputs / Multi-Outputs Wavelength Division Multiplexer

The multiplexing idea explained in section (4.2.1) remains valid, but a number of more output ports were used. Again, the same schematic used for hybrid plasmonic filter that proposed in section (5) with the same design' parameters in terms of dimensions and materials will be used to display the performance of three-inputs / three-output WDM, but after activating the two output ports {port (4) and port (6)} as illustrated in figure (26). Taking into account that all control units appeared in the structure (Control Unit 1, Control Unit 2, and Control Unit 3) are considered in its CROSS state.

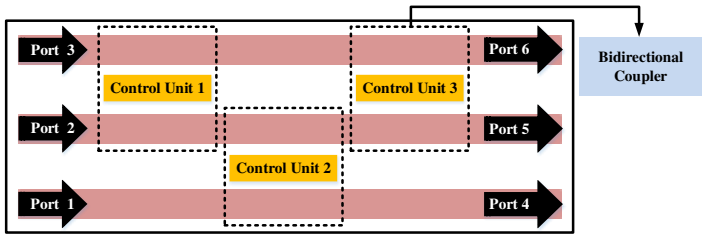

Figure 26: the schematic for three-inputs / three-outputs wavelength division multiplexer.

A polarized light wave of transverse magnetic type is injected at the input ports where each input port carried single wavelength. A wavelength of 1500 nm is injected to (Input 1) port, a wavelength of 1550 nm is injected to (Input 2) port, and a wavelength of 1600 nm is injected to (Input 1) port.

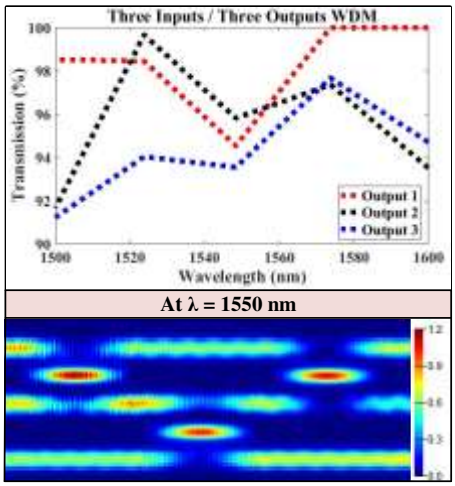

Figure 27: the device' spectrum when input is launched into port (1), and the distribution of electric field (E) intensity for the proposed device.

From following up the performance of the proposed device, shown in figure (27), it is concluded that it distributes the same multiplexed wavelength range at all outputs while keeping the transmission efficiencies values equal on all output ports as well.

6. Modeling of Hybrid Plasmonic 5x5 Switching Matrix

The proposed hybrid plasmonic bidirectional coupler discussed in section (3) is deemed as a base block in modeling other structures. This section discusses modeling of hybrid plasmonic 5x5 switching matrix whose structure shown in figure (28).

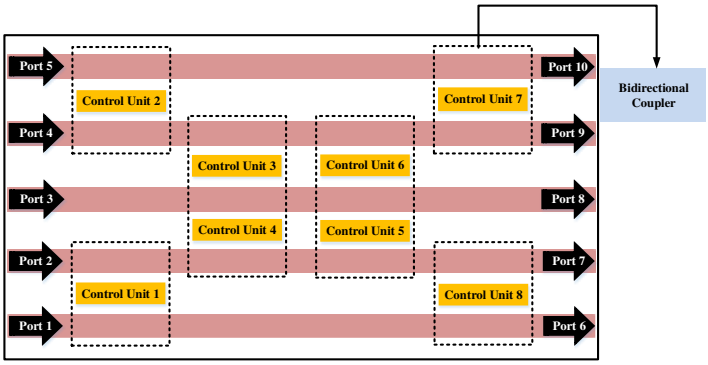

Figure 28: the schematic for hybrid plasmonic 5x5 switching matrix.

Complementing the idea of routing that was applied to the 3x3 switching matrix which was explained in section (5.1), the same way the 5x5 switching matrix works, but more input/output ports have been added, and the number of control units has also been increased. Consequently, the routing conditions, which depend on the states of control units will differ.

The optical power can be injected into any input port {port (1), port (2), port (3), port (4), or port (5)} and it can also exit from any output port {port (6), port (7), port (8), port (9), or port (10)}, depending on the state of the control units. To test the performance of the 5x5 switching matrix and prove its routing function, random cases will be chosen in which to review the process of transferring the optical power from input ports to output ports, as illustrated in table (5).

Table 5: the operation of 5x5 switching matrix according to the state of the control units.

	Control Unit 1	Control Unit 2	Control Unit 3	Control Unit 4	Control Unit 5	Control Unit 6	Control Unit 7	Control Unit 8	
Port 1	CROSS	BAR	BAR	BAR	BAR	BAR	BAR	BAR	**Port 7**
Port 2	CROSS	BAR	BAR	BAR	BAR	BAR	BAR	BAR	**Port 6**
Port 3	BAR	BAR	CROSS	BAR	BAR	BAR	BAR	BAR	**Port 9**
Port 4	BAR	CROSS	BAR	BAR	BAR	BAR	BAR	BAR	**Port 10**
Port 5	BAR	CROSS	CROSS	BAR	CROSS	BAR	BAR	BAR	**Port 7**

All power transmission cases shown in tables (5) have been displayed and the device performance can be analyzed using equation (7). Hint; m = (1, 2, 3, 4, and 5) and n = (6, 7, 8, 9, 10). Figures from (29) to (31) illustrate the obtained transmission efficiencies over the selected wavelength range (1500-1600) nm.

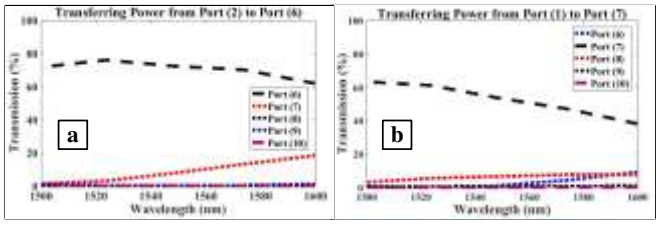

Figure 29: the device' spectrum for a) transferring power from port (2) to port (6), and b) transferring power from port (1) to port (7) as a function of wavelength.

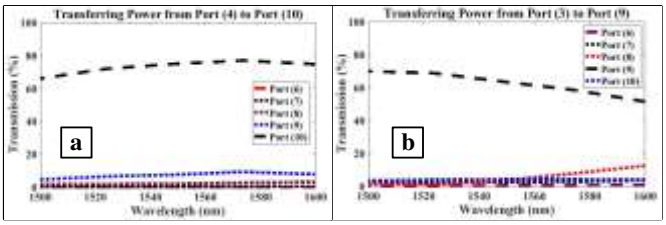

Figure 30: the device' spectrum for a) transferring power from port (4) to port (10), and b) transferring power from port (3) to port (9) as a function of wavelength.

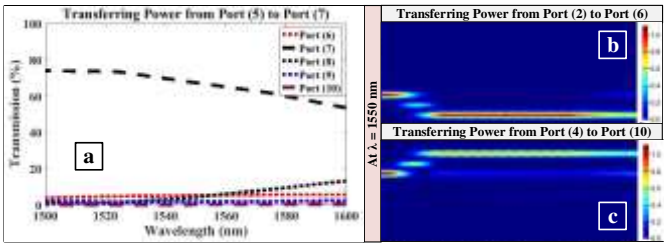

Figure 31: a) the device' spectrum for a) transferring power from port (5) to port (7) as a function of wavelength, b) and c) the field distribution over the device at a wavelength of 1550 nm.

The obtained data at the wavelength of 1550 nm are utilized to set a validation with the data proposed at research [26]. The common design elements utilized in the comparison are: thickness of noble metal = 100 nm, height of ITO layer = 20 nm, coupling gap = 150 nm, SOI strip waveguide = 400x340 nm^2, MOS waveguide = 275x340 nm^2, resistance = 500 Ω, and biasing voltage = 4 volts. Hint; the two design used the same technology.

A comparison between the obtained results in this work with their counterparts in reference [24] is proposed in table (6). Obviously, the transmission efficiencies proposed in research [24] are approximately less than 45 % at the desired output ports, and they are approximately less than 10 % at the undesired output ports. But the transmission values that obtained in this work are approximately more than 60 % at the desired output ports and they are approximately less than 10 % at the undesired output ports.

Table 6: a comparison between some properties of two different devices.

Parameter	Present work	Reference [24]
Coupling Length (μm)	8	8.9
No. of Oxide Layers	One layer	Two layers
Thickness of ITO	20 nm per layer	16 nm per layer
Metal Layer	Silver	Gold
Transmission At the desired output port	≥ 60%	≤ 45 %
Transmission At the undesired output port	≤ 10%	≤ 10%

7. Modeling of Hybrid Plasmonic Logic Gate Circuit

To complement the set of logic gates announced during this work, two different gates will be presented, namely OR and NAND logic gates, using the same design, but with a different operating method, and this is an application of the multi-use device technology that was previously mentioned. The suggested design used for modeling the two logic gates that proposed in this section is shown in figure (32). The ports that are used in the proposed design are 1, 2, and 3, while the rest of the ports are inactive.

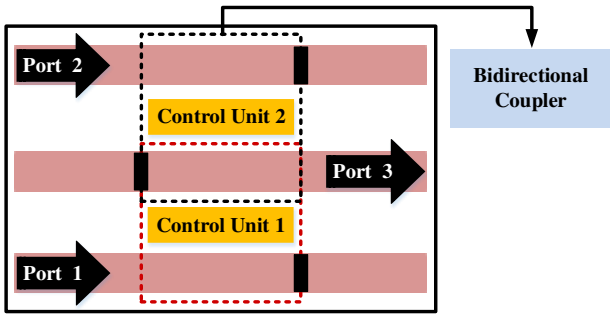

Figure 32: the 2D- XY view of the schematic used for both of the OR and NAND logic gates.

7.1. Modeling of Hybrid Plasmonic OR Logic Gate

The symbol and the truth table of OR logic gate is illustrated in figure (33). As is evident from the figure, there are four inputs for the gate, two inputs representing the control signals, and the other two inputs representing the main input signals.

As for OR gate, its operation depends on installing the control units on the CROSS states, or in other words, set the two control signals (X and Y) on zero volts, while the change takes place in the main input signals (A and B) as illustrated in the truth table shown in figure (33).

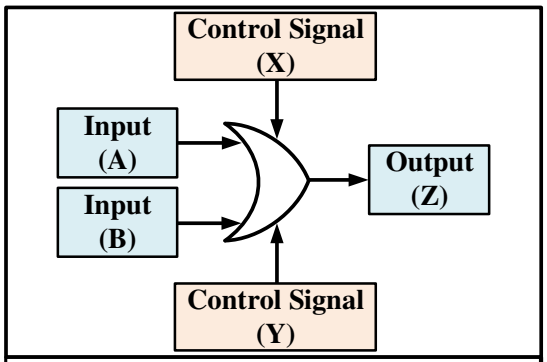

The truth table of OR gate

X	Y	A	B	Z
ON	ON	OFF	OFF	OFF
ON	ON	OFF	ON	ON
ON	ON	ON	OFF	ON
ON	ON	ON	ON	ON

Figure 33: the symbol and the truth table of hybrid plasmonic OR logic gate.

Figure (34) shows the performance of the logic gate by using the transmission value, which is calculated from equation (11)

$$\textbf{Transmission}\ (\%) = 100 * \left(\frac{Power_{Port\,(3)}}{Power_{Port\,(1,\ or\ 2)}}\right) \qquad (11)$$

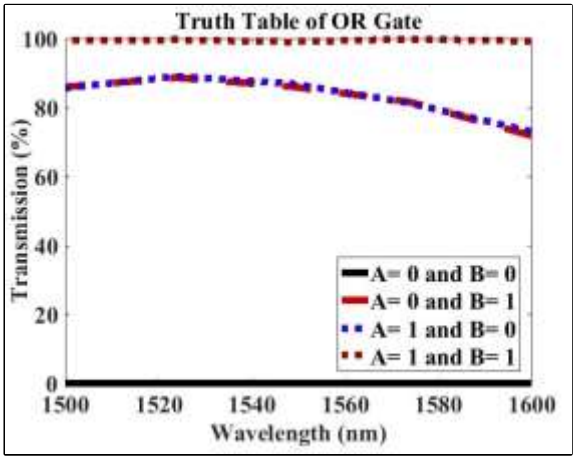

Figure 34: the OR gate performance in terms of transmission as a function of wavelength.

When the two control signals are on the zero-volt mode (OFF state), the two main input signals (A and B) are changed according to the truth. Whereas, the output gives Logic 1 in three cases with a transmission value of more than 80% at the telecommunication wavelength, while the fourth case has a transmission value equals to zero.

7.2. Modeling of Hybrid Plasmonic NAND Logic Gate

The symbol and the truth table of NAND logic gate is illustrated in figure (35). Here, the operation depends on installing the two main input signals (A and B) on the ON states, while the change takes place in the input control signals (X and Y) as illustrated in the truth table shown in figure (35).

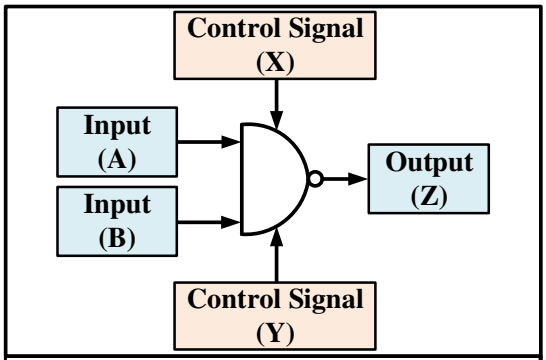

The truth table of NAND gate

A	B	X	Y	Z
ON	ON	OFF	OFF	ON
ON	ON	OFF	ON	ON
ON	ON	ON	OFF	ON
ON	ON	ON	ON	OFF

Figure 35: the symbol and the truth table of hybrid plasmonic NAND logic gate.

The performance of the NADN logic gate is illustrated in figure (36) in terms of the transmission efficiency, which is calculated from equation (8). Hint; CROSS state is equivalent to Logic 0, and BAR state is equivalent to Logic 1.

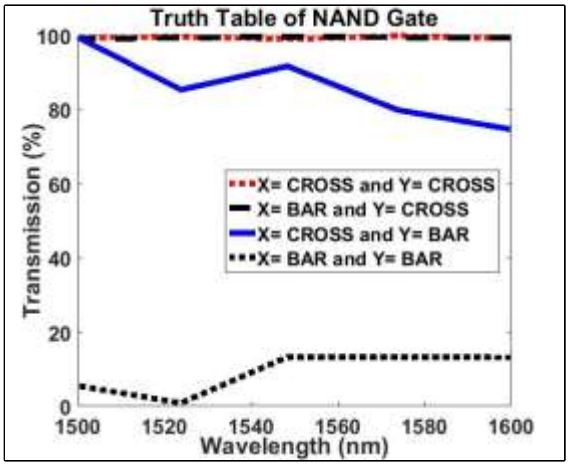

Figure 36: the NADN gate performance in terms of transmission as a function of wavelength.

Conclusion

This work proposed modeling and optimizing the performance of hybrid plasmonic bidirectional coupler which is used as a basic building block in modeling more complex devices such as filter, wavelength division multiplexer, logic gates and switching matrix with a help of an active material (indium tin oxide) that has an electrically-adjustable permittivity. All the proposed devices satisfied high transmission efficiencies at the desired output ports over a suitable wavelength range. The components would be useful in the optical interconnect networks, photonic integrated circuits and signal processing system.

Declarations

- Funding: Not applicable.
- Conflicts of interest/Competing interests: Not applicable.
- Availability of data and material: are available.
- Code availability: is available.
- Authors' contributions: Participate in moral support, help with theoretical background and review research to give feedback.
- Ethics approval: approved.
- Consent to participate: accept.
- Consent for publication: accept.

References

1) Shuai Sun, Ruoyu Zhang, Jiaxin Peng, Vikram K. Narayana. "MO detector (MOD): a dual-function optical modulator-detector for on-chip communication," Opt. Express, Vol. 26, PP. 8252–8259, 2018.

2) Mandeep Singh, Sanjeev Kumar, Raghu wanshi, and T. Srinivas, "Nanophotonic on-chip hybrid plasmonic electro-optic modulator with phase change materials," Physics Letters A (Elsevier), Vol. 383, PP. 3196-3199, 2019.

3) D. A. Miller, "Attojoule optoelectronics for low-energy information processing and communications," J. Lightw. Technol., Vol. 35, PP. 346–396, 2017.

4) Zhengying Xu and Xiaohan Sun, "Ultra-broadband TE-pass polarizer based on hybrid plasmonic-assisted contra-directional couplers," J. Opt. Soc. Am. B, Vol. 37, PP. 251-256, 2020.

5) Rami A. Wahsheh1, and Mustafa A. G. Abushagur, "Experimental and theoretical investigations of an air-slot coupler between dielectric and plasmonic waveguides," Optics Express, Vol. 24, PP. 8237–8242, 2016.

6) R. Wahsheh and M. Abushagur, "Switchable plasmonic routers controlled by external magnetic fields by using magneto-plasmonic waveguides," Scientific Reports, Vol. 18, PP. 10584–10592, 2018.

7) Zhixun, Liang Chuanpei, Xu Aijun, Zhu Shehui, Du, Cong, Hu, "Hybrid photonic-plasmonic electro-optic modulator for optical ring network-on-chip," Optik (Elsevier), Vol., PP., 2020. (doi.org/10.1016/j.ijleo.2020.164503).

8) Dutta, A., Kildishev, A. V., Shalaev, V. M., Boltasseva, A. & Marinero, E. E. "Surface-plasmon opto-magnetic field enhancement for all-optical magnetization switching," Opt. Mater. Express, Vol. 7, PP. 4316–4327, 2017.

9) Zhou, W., Huang, X. "Active control of optical signals in the plasmonic waveguides," Int. J. Electr. Energy, Vol. 1(4), PP. 304–307, 2013.

10) J. Chee, S. Zhu, and G. Q. Lo, "CMOS compatible polarization splitter using hybrid plasmonic waveguide," Opt. Express, Vol. 20(23), PP. 25345–25355, 2012.

11) S. K. Pickus, S. Khan, C. Ye, Z. Li, and V. J. Sorger, "Silicon plasmon modulators: Breaking photonic limits," *IEEE Photonic Soc.*, Vol. 27, PP. 4–10, 2013.

12) Mandeep Singh, Sanjeev Kumar, Raghu wanshi, and T. Srinivas, "Nanophotonic on-chip hybrid plasmonic electro-optic modulator with phase change materials," Physics Letters A (Elsevier), Vol. 383, PP. 3196-3199, 2019.

13) F. Lou, D. Dai, and L. Wosinski, "Ultra-compact polarization beam splitter based on a dielectric-hybrid plasmonic-dielectric coupler, Opt. Lett. Vol. 37(16), PP. 3372–3374, 2012.

14) Jackel, H., Bona, G.L., Hafner, C. "Ultrafast, compact, and energy efficient all-optical switches based on a saturable absorbing cavity," IEEE J. Quantum Electron, Vol. 50(12), PP. 1–10, 2014.

15) Mahsa Babaei, Abbas Zarifkar, and Mehdi Miri, "Compact and broadband 2 × 2 optical switch based on hybrid plasmonic waveguides and curved directional couplers," Applied Optics, Vol. 59, PP. 975-984, 2020.

16) Maithem S. Jaber, Shelan K. Tawfeeq, and Raad S. Fyath, "Design Investigation of 4 × 4 Nonblocking Hybrid Plasmonic Electrooptic Switch," photonics, Vol. 6, PP. 1–21, 2019.

17) Lin Jin, Long Wen, Li Liang, Qin Chen and Yunfei Sun, "Polarization-Insensitive Surface Plasmon Polarization Electro-Absorption Modulator Based on Epsilon-Near-Zero Indium Tin Oxide," Nano Lett., Vol. 18, PP. 13–39, 2018.

18) Aya Amer, Mohamed M Badr, and Mohamed A Swillam, "VO2/ITO Hybrid Plasmonic High Performance Electro-Optical Modulator," Optical Society of America, Vol. 59, PP., 2018. (https://doi.org/10.1364/FIO.2018.JW3A.96).

19) Shin, Wonseok, Fan, Shanhui, "Choice of the perfectly matched layer boundary condition for frequency domain Maxwell's equations solvers," J. Comput. Phys., Vol. 231, PP. 3406–3431 (2012).

20) E. Palik, "Handbook of Optical Constants of Solids," New York: Academic, 1985.

21) J. Simmons and K. S. Potter, "Optical Materials," CA: San Diego, Academic Press, 2000.

22) Chenran Ye, Ke Liu, Richard A. Soref, and Volker J. Sorger, "A compact plasmonic MOS-based 2×2 electro-optic switch," Nanophotonics, Vol. 4, PP. 261–268, 2015.

23) Viktoriia E. Babicheva, Andrei V. Lavrinenko, "Plasmonic modulator optimized by patterning of active layer and tuning permittivity," Optics Communications, Vol. 285, PP. 5500-5507, 2012.

24) Shuai Sun, Vikram K. Narayana, "Hybrid Photonic-Plasmonic Nonblocking Broadband 5 × 5 Router for Optical Networks," IEEE Photonics Journal, Vol. 10, PP. 1109–1119, 2018.

25) Viktoriia E. Babicheva, Alexandra Boltasseva, and Andrei V. Lavrinenko, "Transparent conducting oxides for electro-optical plasmonic modulators," Nanophotonics, Vol. 4, PP. 165–185, 2015.

26) P. Xu, J. Zheng, J. K., Doylend, and Arka M. " Low-Loss and Broadband Nonvolatile Phase-Change Directional Coupler Switches," ACS Photonics, Vol. 6, PP. 553–557, 2019.

Figures

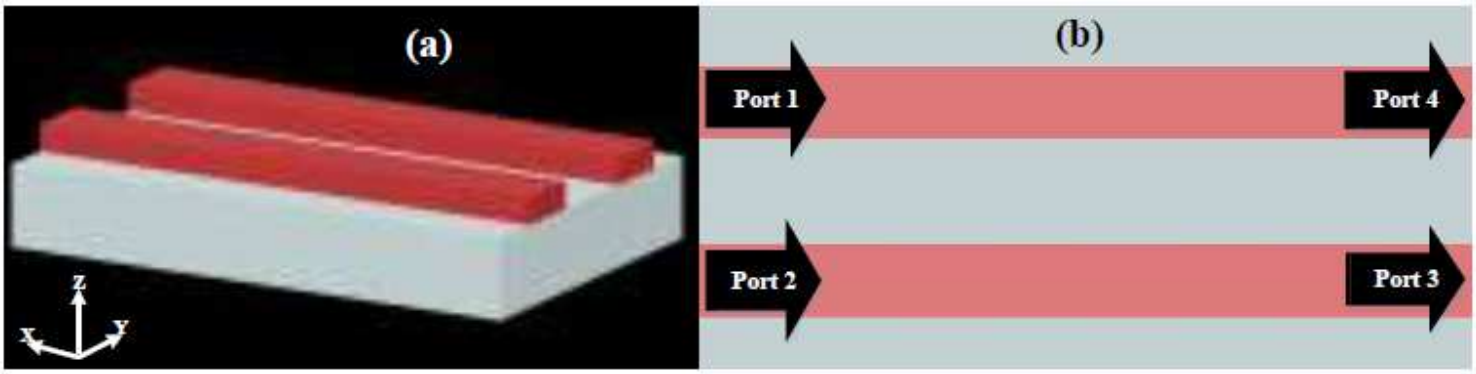

Figure 1

the schematic of base unit (two SOI strip waveguides); a) 3D- view, and b) 2D- XY view.

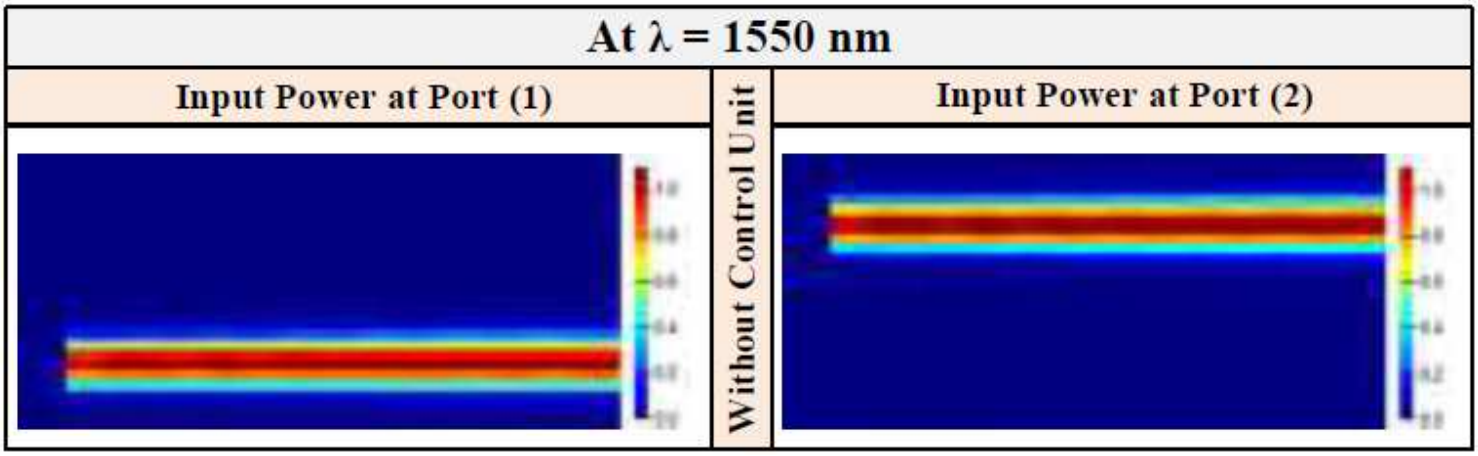

Figure 2

the distribution of electric field (E) intensity for the base unit (two SOI strip waveguides) without control unit.

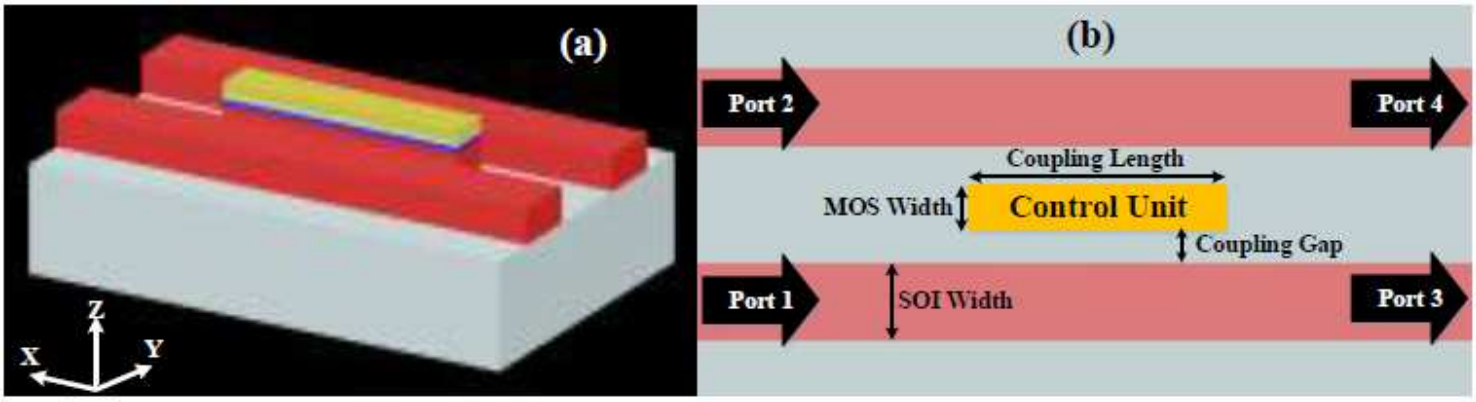

Figure 3

the schematic of the proposed bidirectional coupler after adding the control unit; a) 3D- view, and b) 2D-XY view.

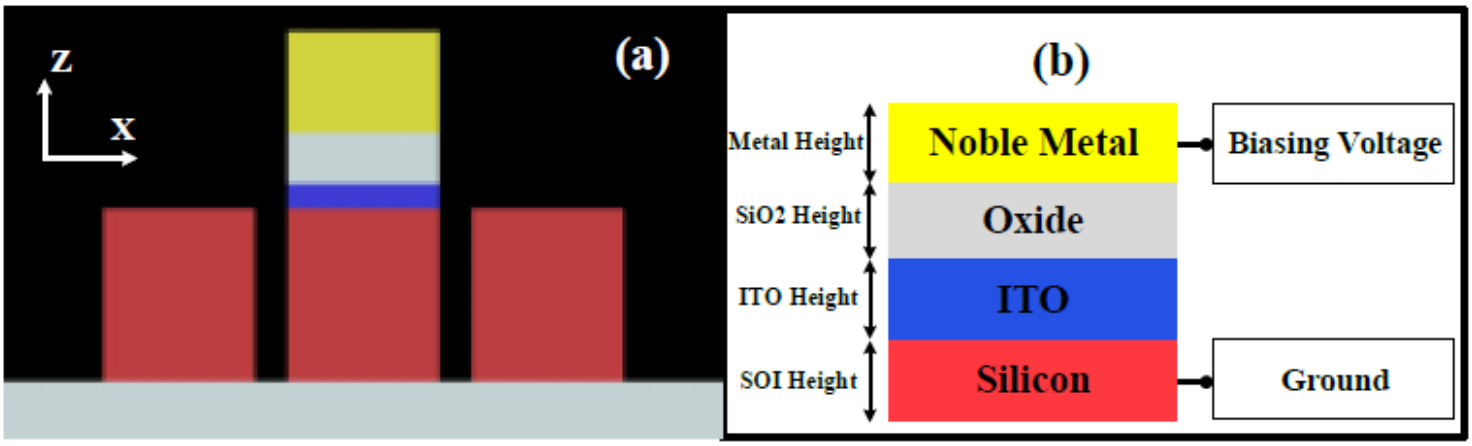

Figure 4

a) the 2D- XZ view of bidirectional coupler, and b) the construction of MOS waveguide.

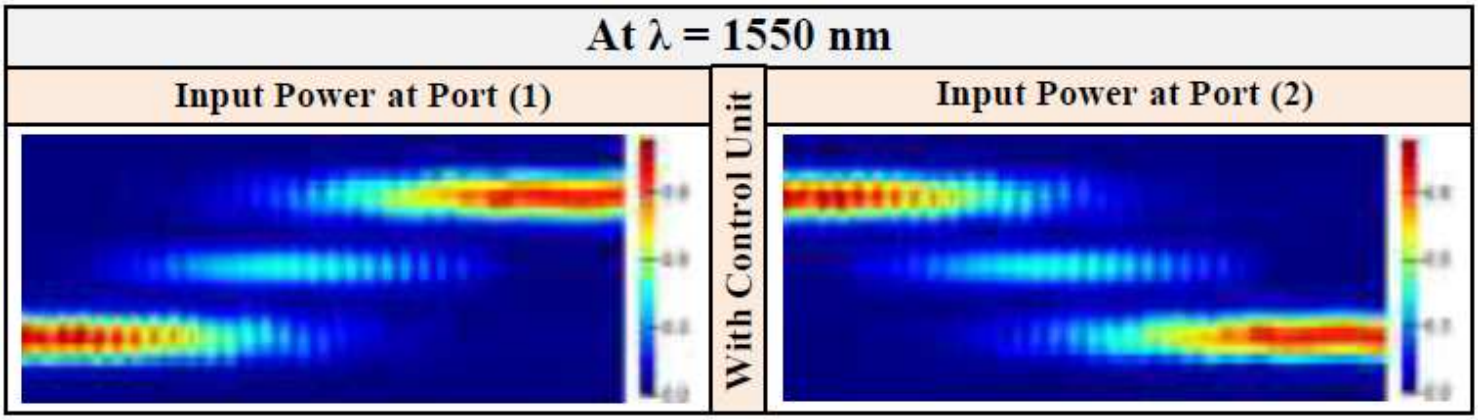

Figure 5

the distribution of electric field (E) intensity for the proposed bidirectional coupler after adding the control unit.

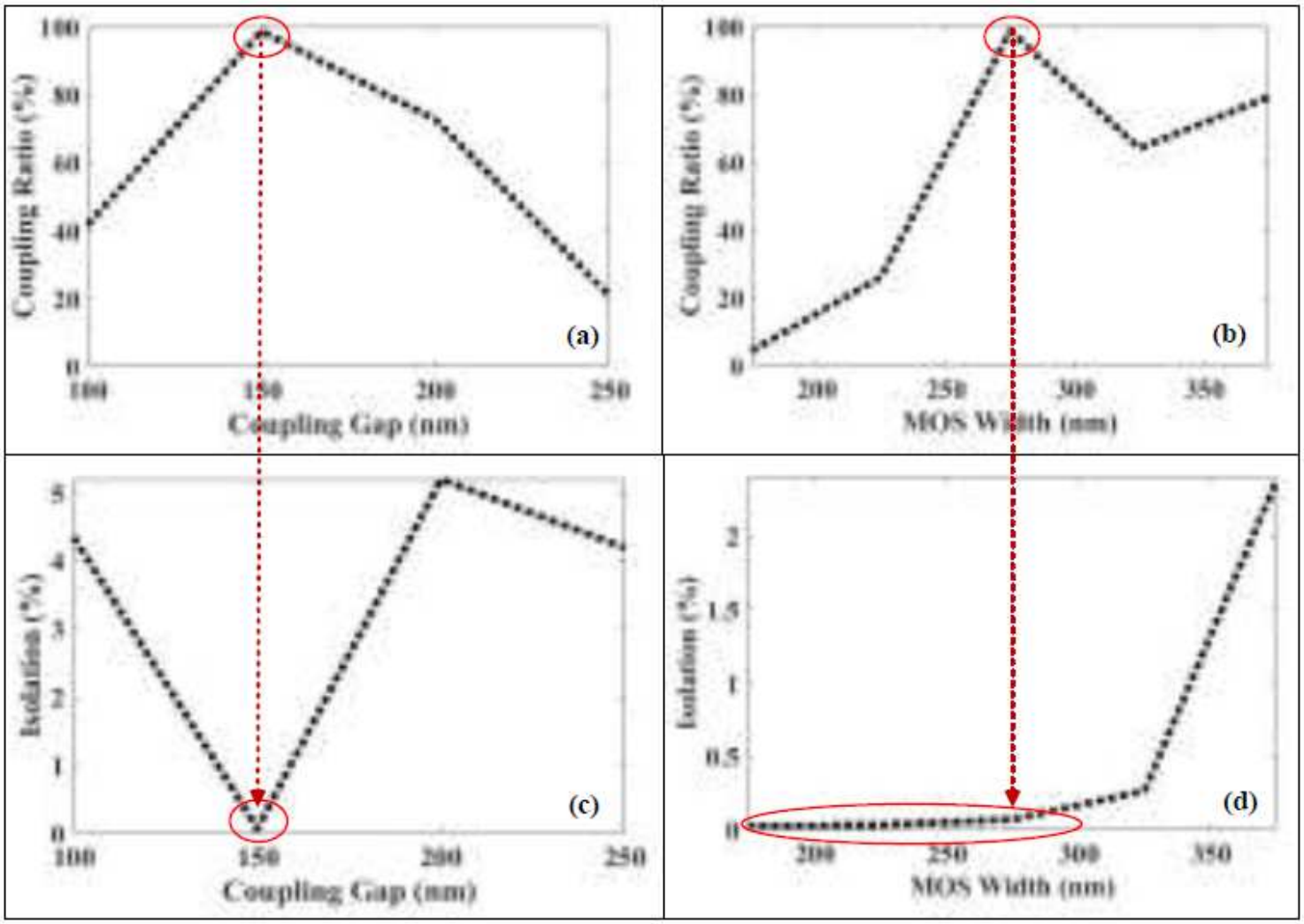

Figure 6

the analyzed results of coupling ratio (CR) as a function of a) the gap width and b) the MOS waveguide width at the optical communication wavelength (1550 nm).

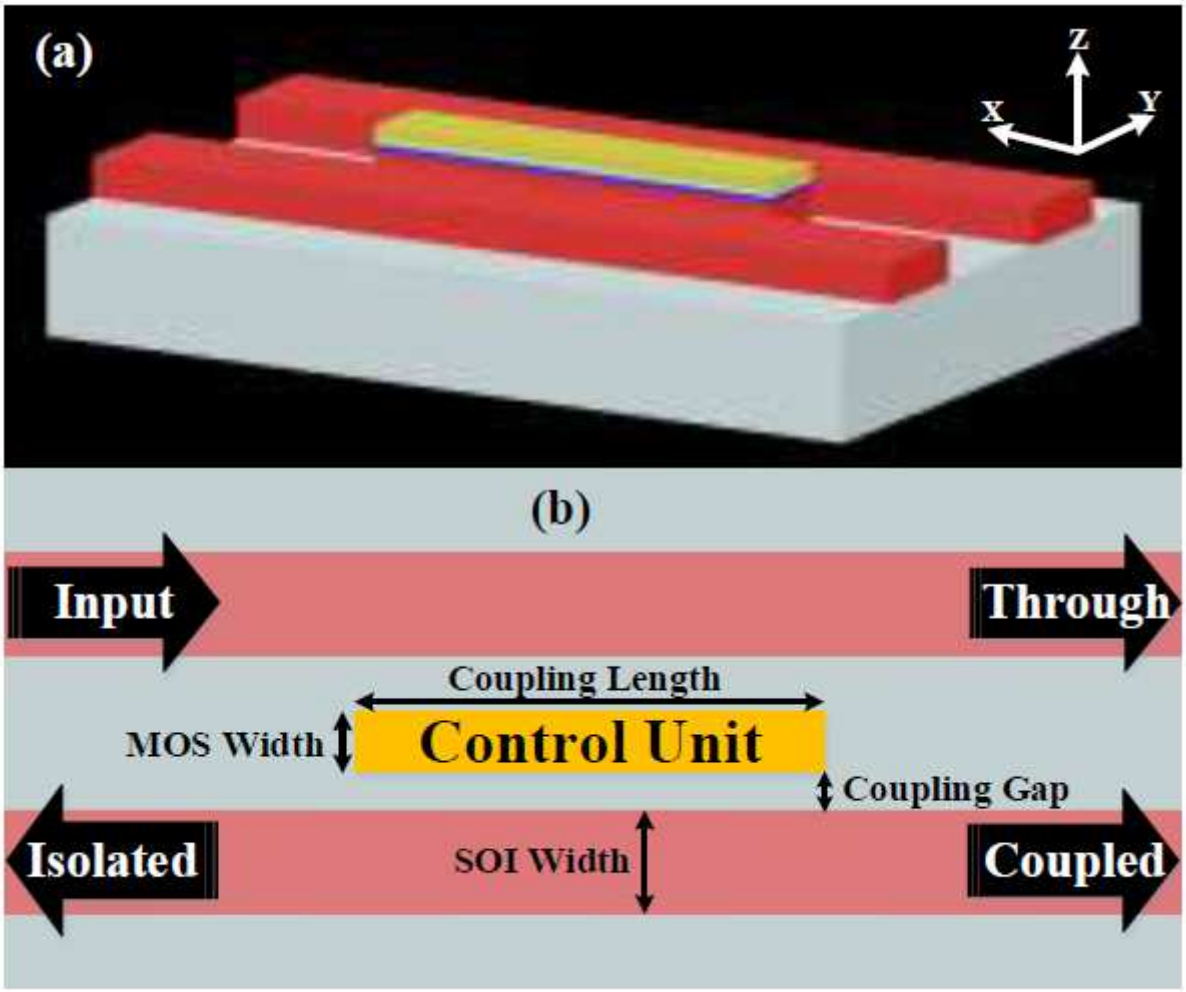

Figure 7

a) 3D- view, and b) 2D- XY view of hybrid plasmonic 2x2 bidirectional coupler.

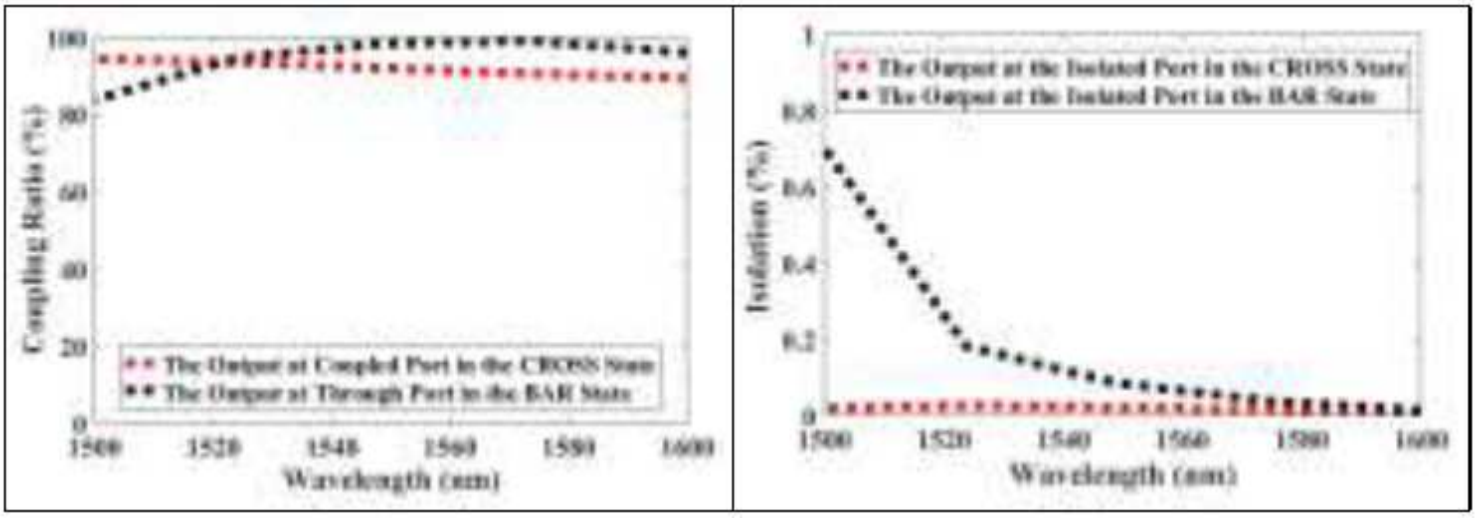

Figure 8

the analyzed results of coupling ratio (CR) and isolation as a function of wavelength.

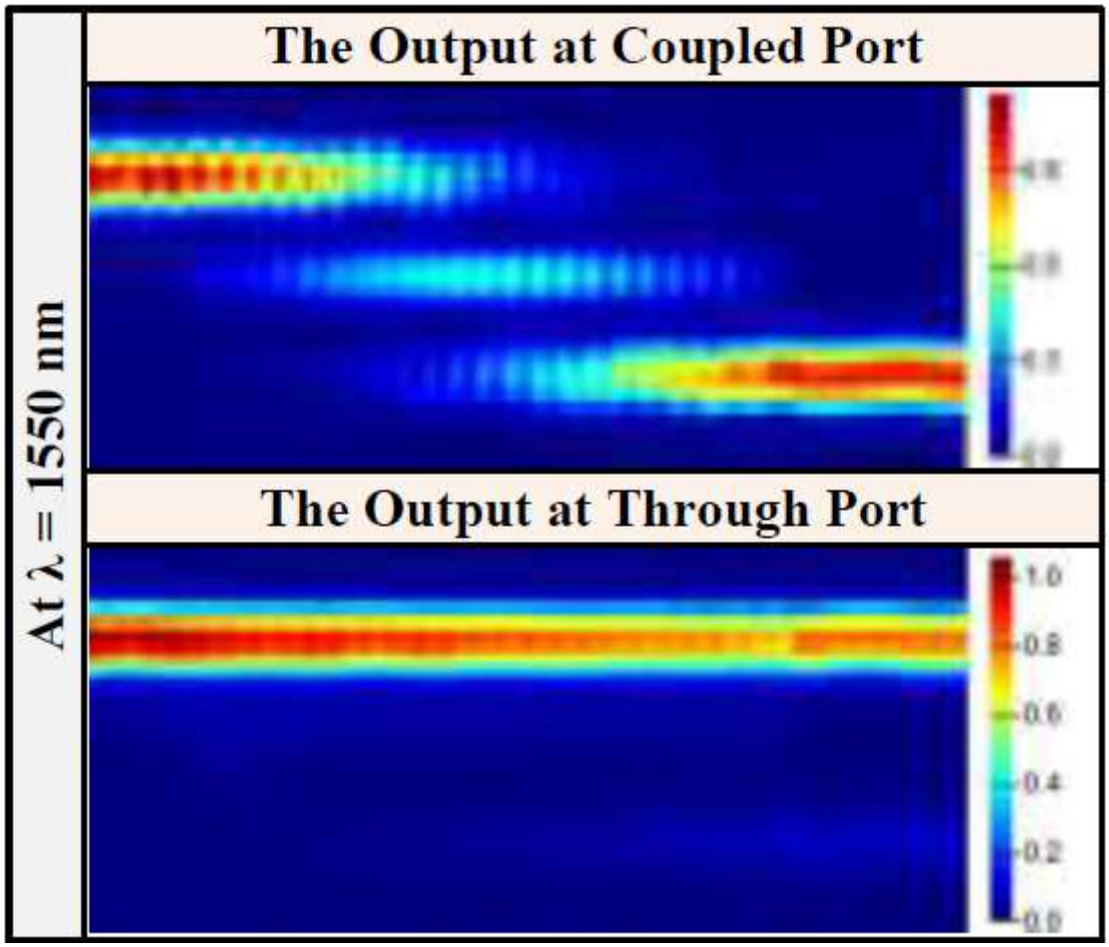

Figure 9

the distribution of electric field (E) intensity at Coupled / Through states of the proposed bidirectional coupler.

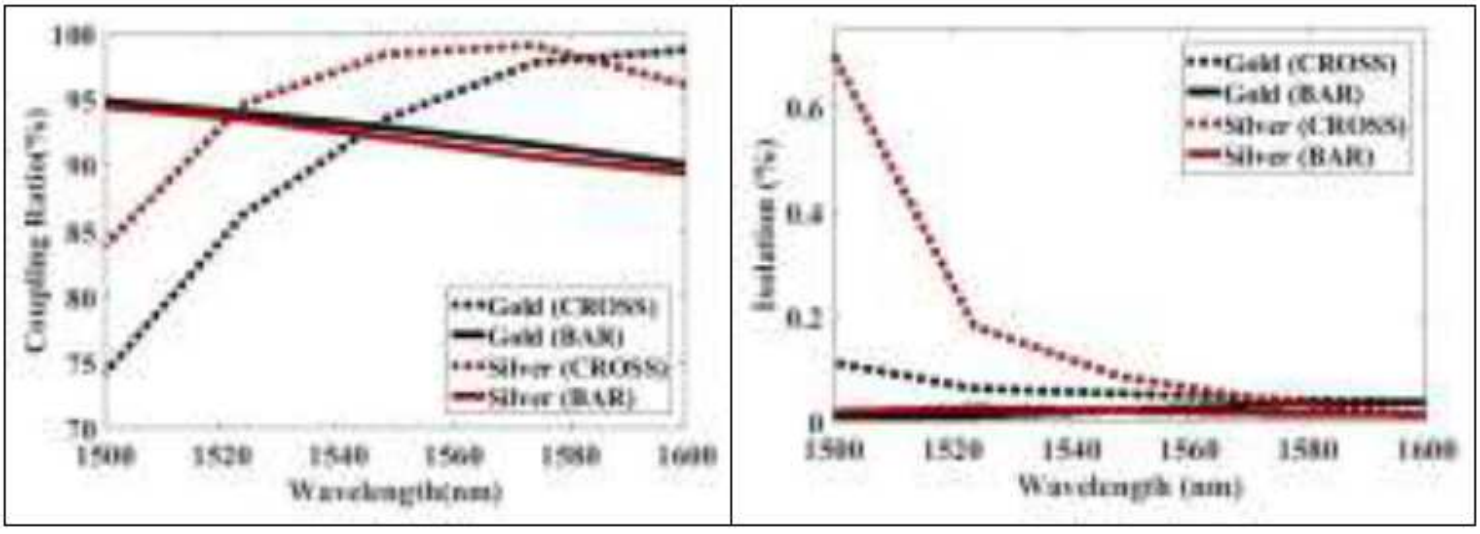

Figure 10

a comparison between the coupler's performance in terms of coupling ratio and isolation in the case of using gold and silver as noble metals over a specified range of wavelengths.

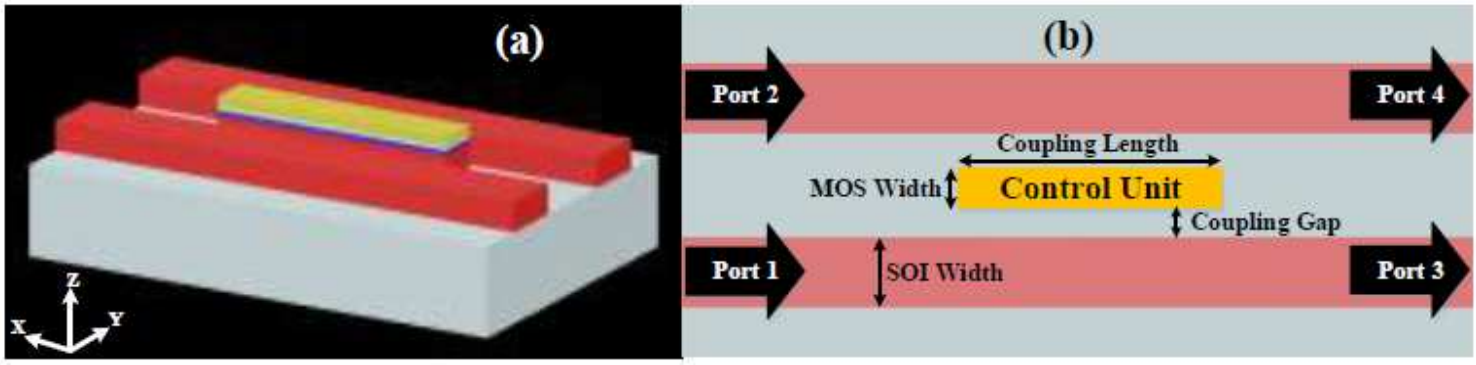

Figure 11

a) 3D- view, and b) 2D- XY view of hybrid plasmonic 2x2 electro-optic switch.

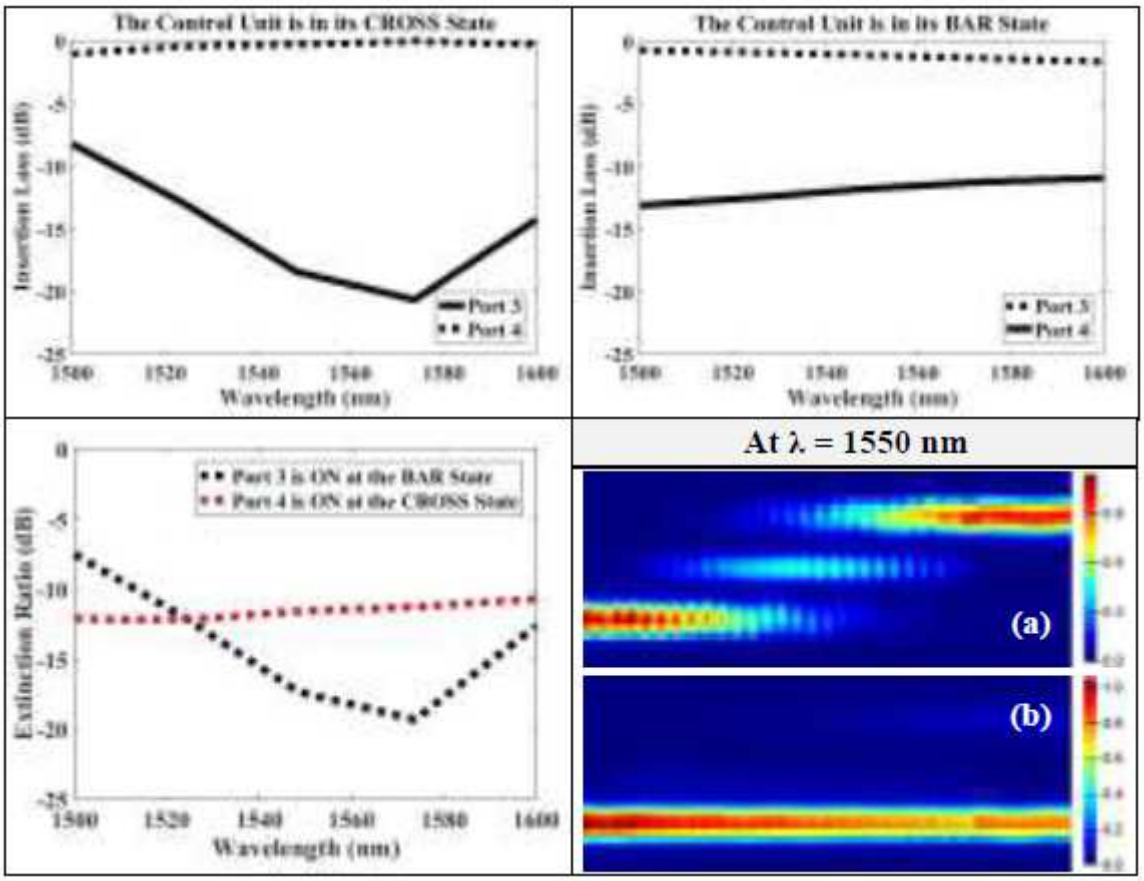

Figure 12

the switch performance in terms of insertion loss and extinction ratio at the two states of control unit. the distribution of electric field (E) intensity at a) CROSS state and b) BAR state over the switch in the XY plane.

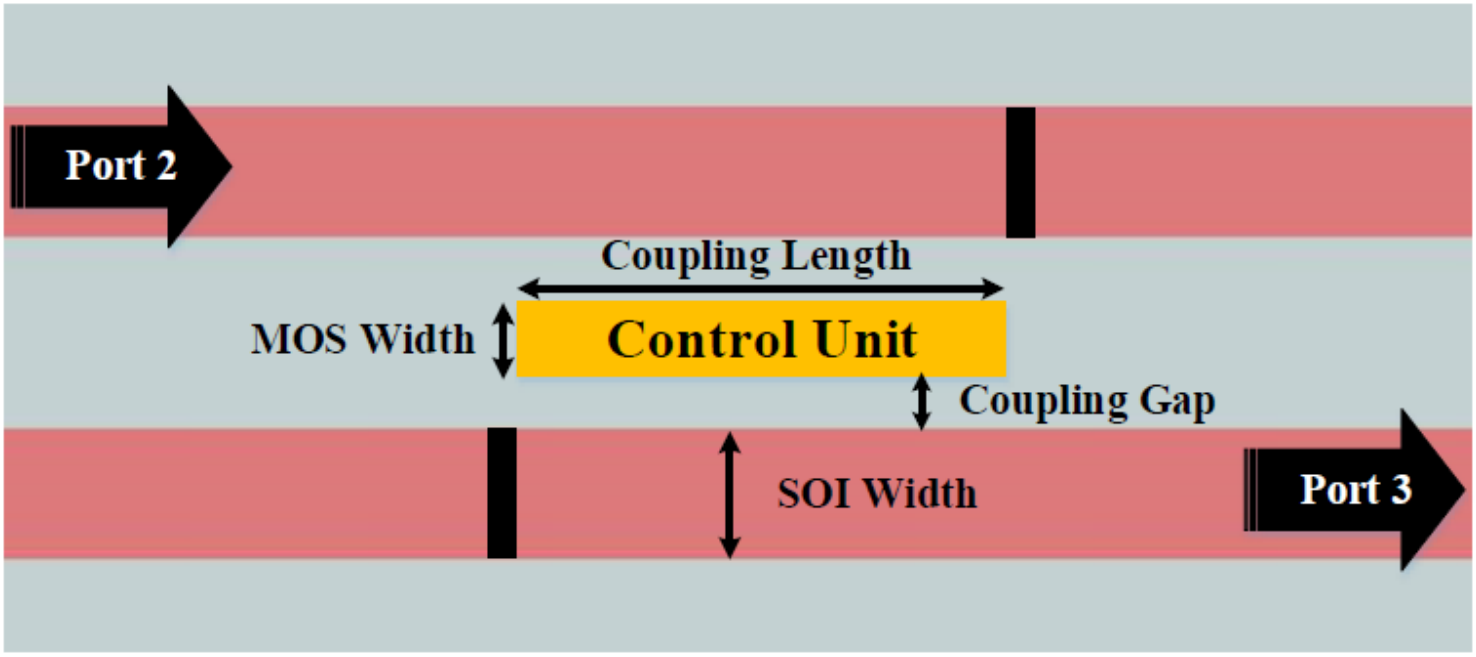

Figure 13

the 2D- XY view of hybrid plasmonic NOT logic gate.

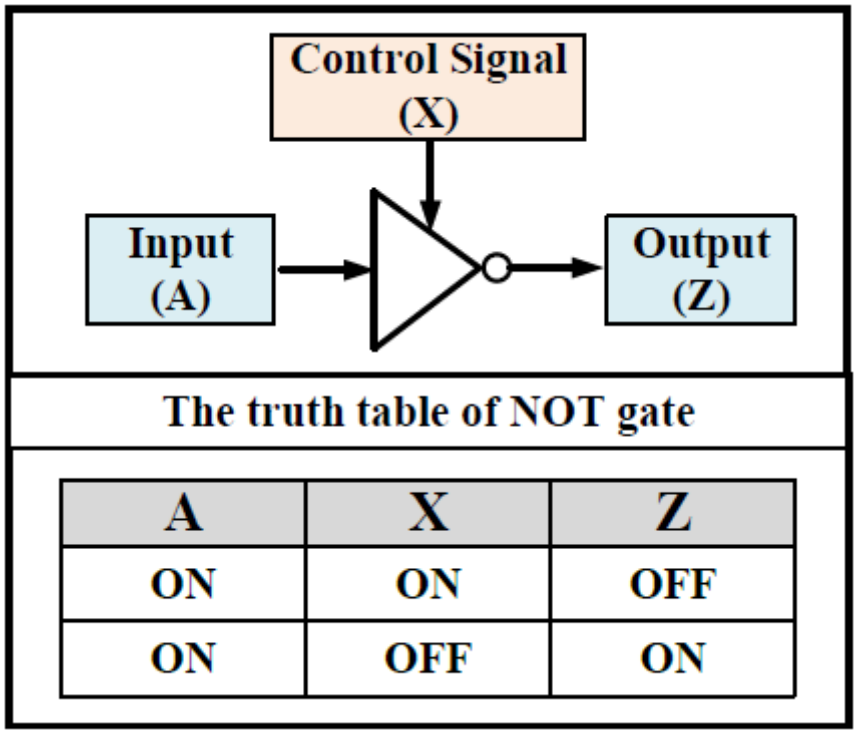

The truth table of NOT gate

A	X	Z
ON	ON	OFF
ON	OFF	ON

Figure 14

the symbol and the truth table of hybrid plasmonic NOT logic gate.

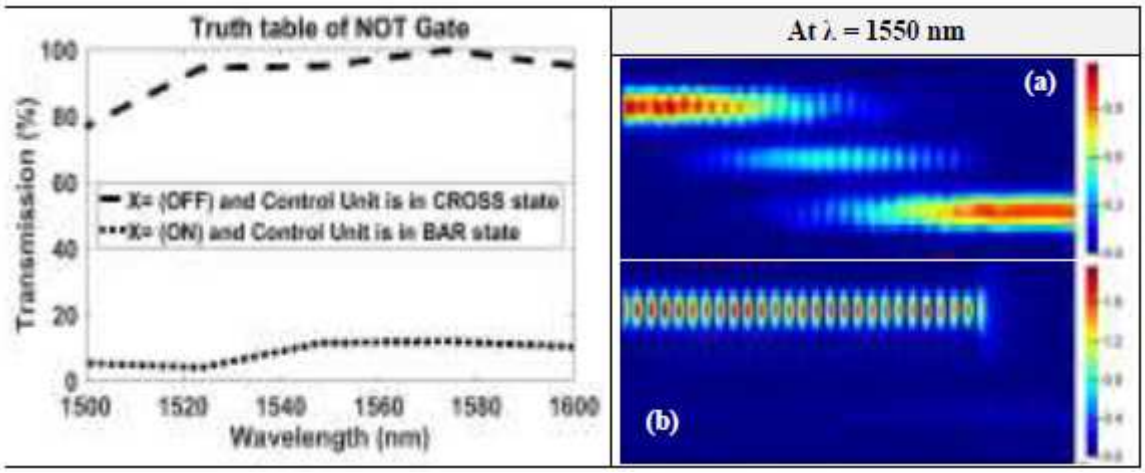

Figure 15

the NOT gate performance in terms of transmission as a function of wavelength, and the distribution of electric field (E) intensity at the two states of truth table over the switch in the XY plane a) X=OFF and Z=ON, b) X=ON and Z=OFF.

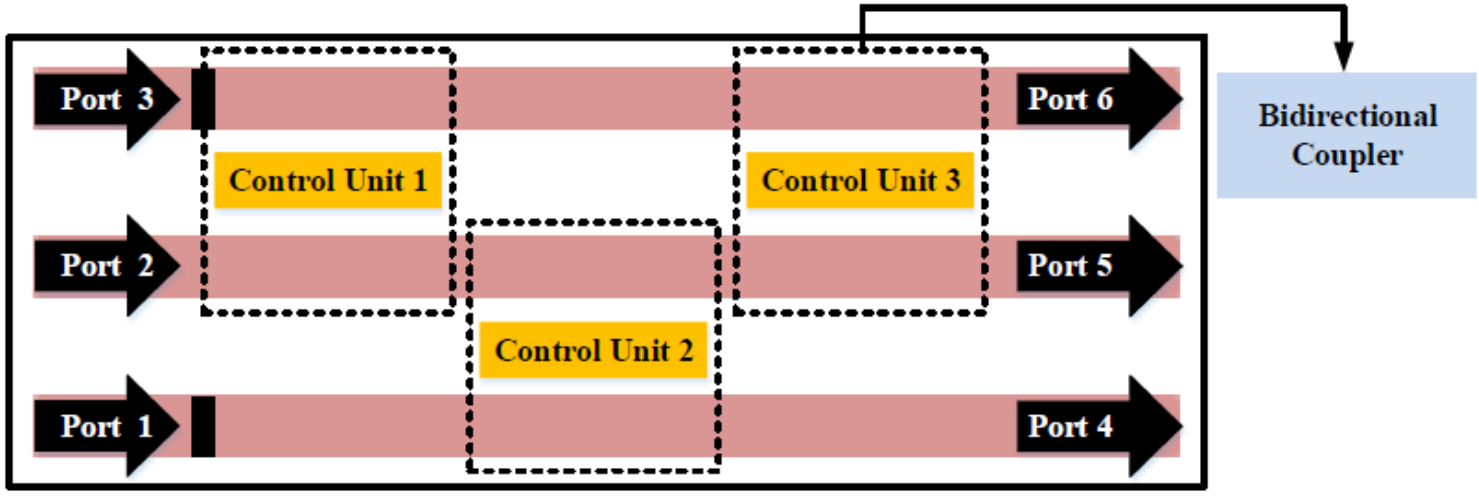

Figure 16

the 2D- XY view of hybrid plasmonic filter.

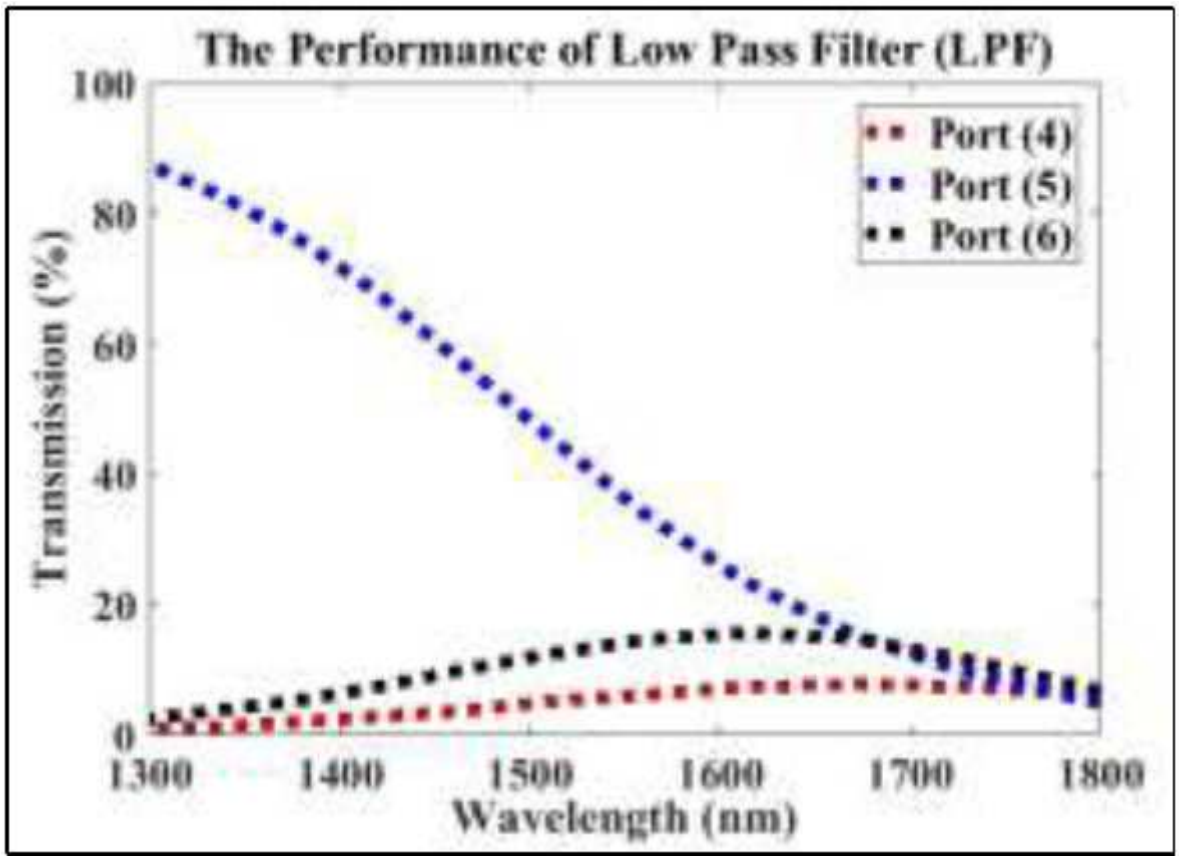

Figure 17

the LPF' performance in terms of transmission as a function of wavelength.

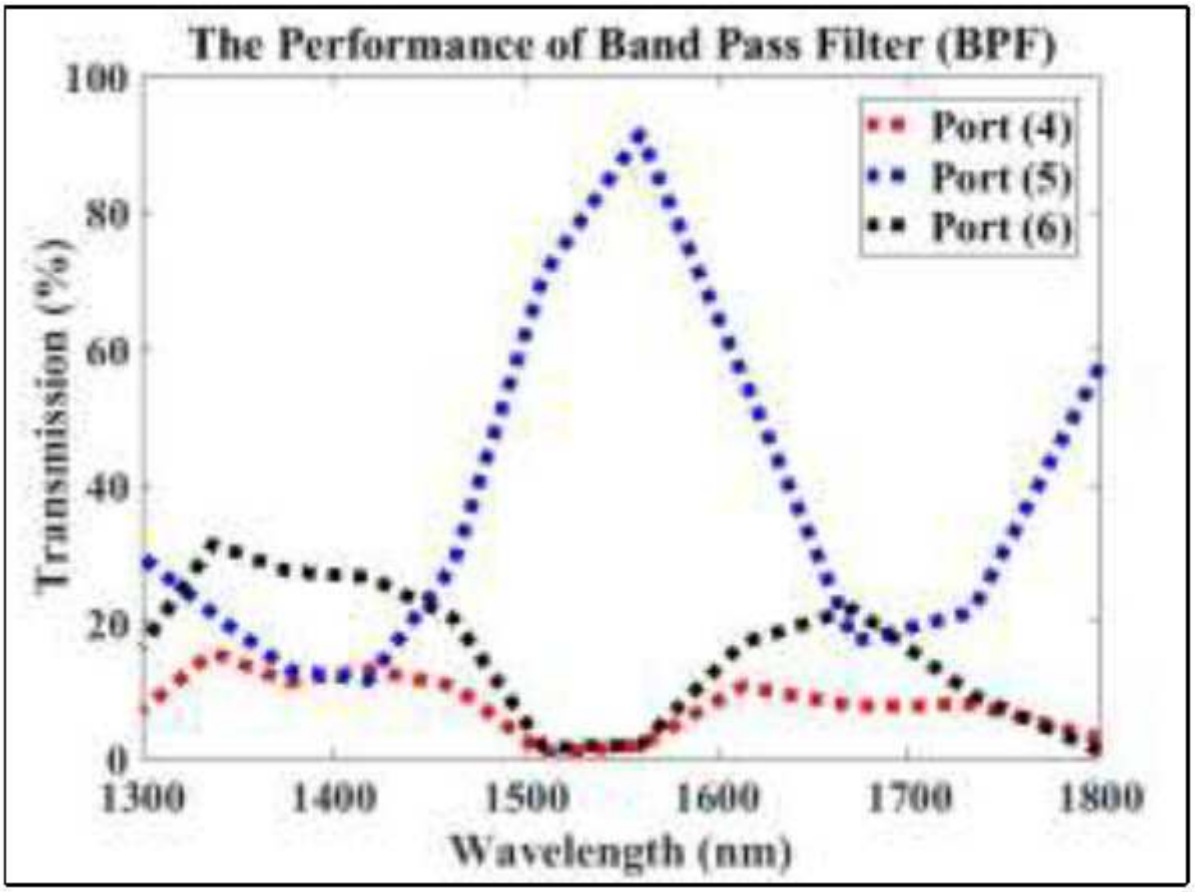

Figure 18

the BPF' performance in terms of transmission as a function of wavelength.

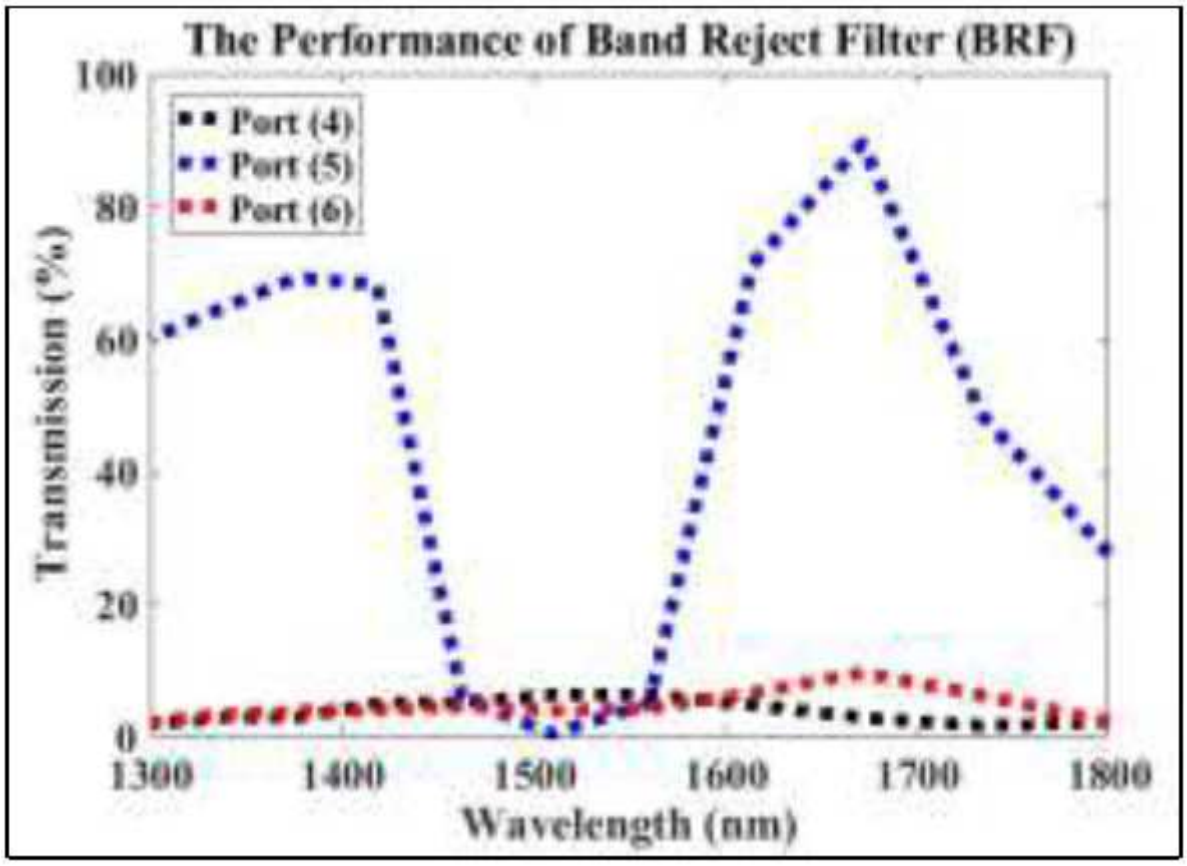

Figure 19

the BRF' performance in terms of transmission as a function of wavelength.

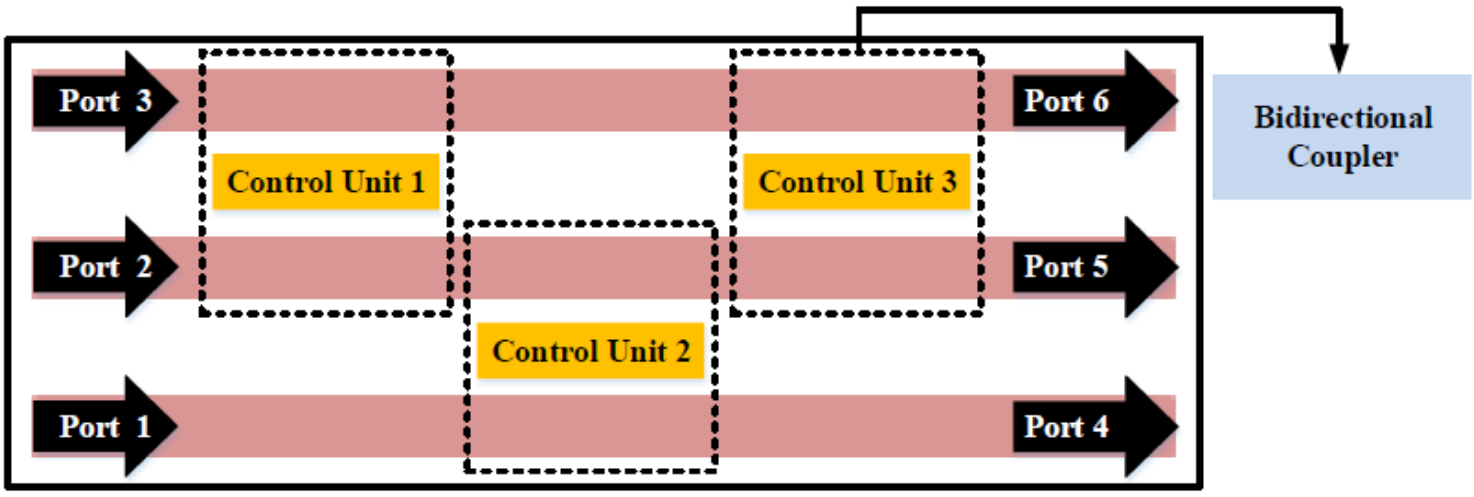

Figure 20

the 2D- XY view of hybrid plasmonic 3x3 switching matrix.

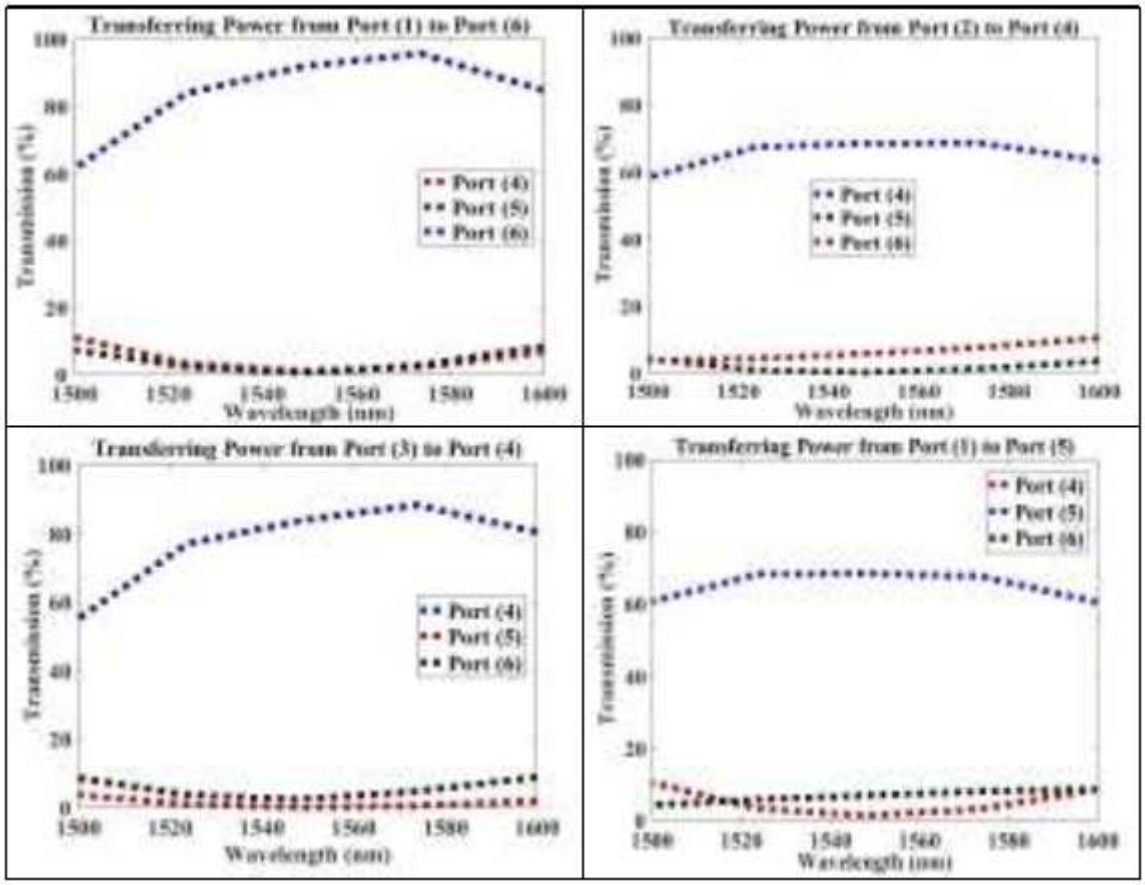

Figure 21

the 3x3 switching matrix' performance in terms of transmission as a function of wavelength.

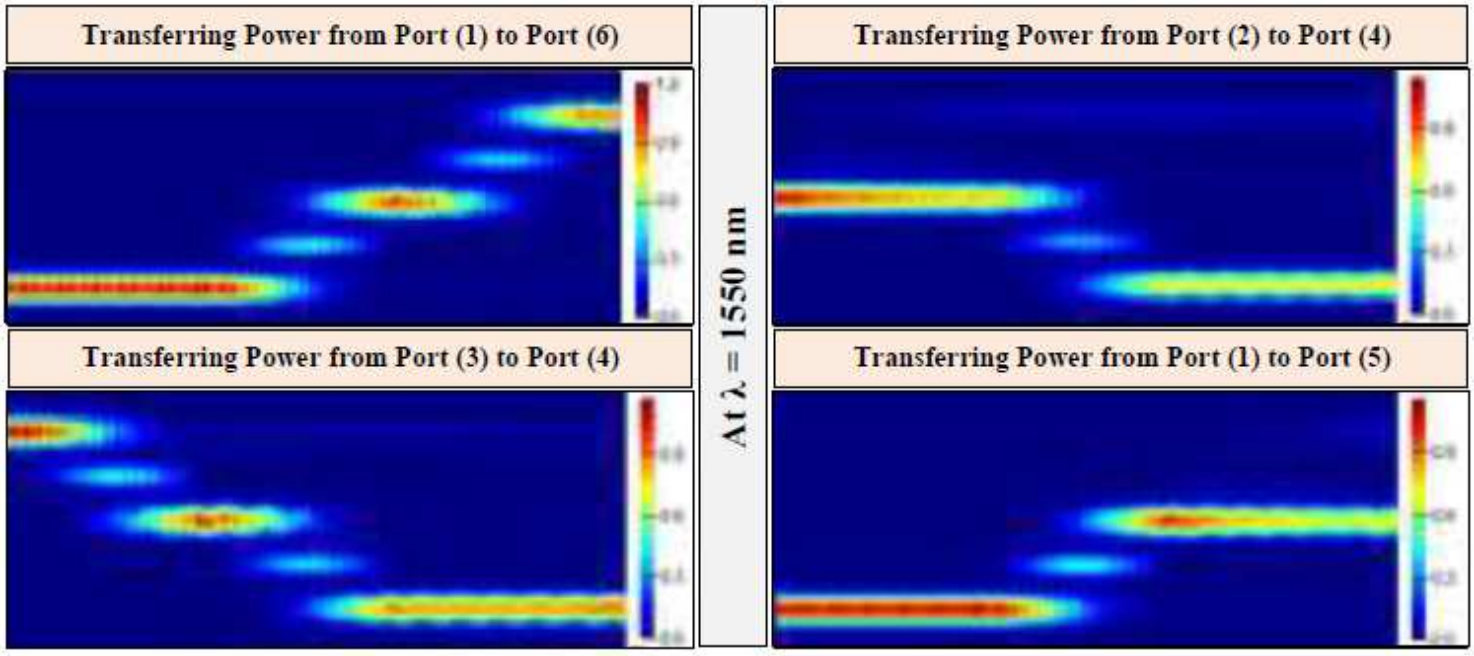

Figure 22

the electric field intensity distribution for 3x3 switching matrix' performance at the telecommunication wavelength.

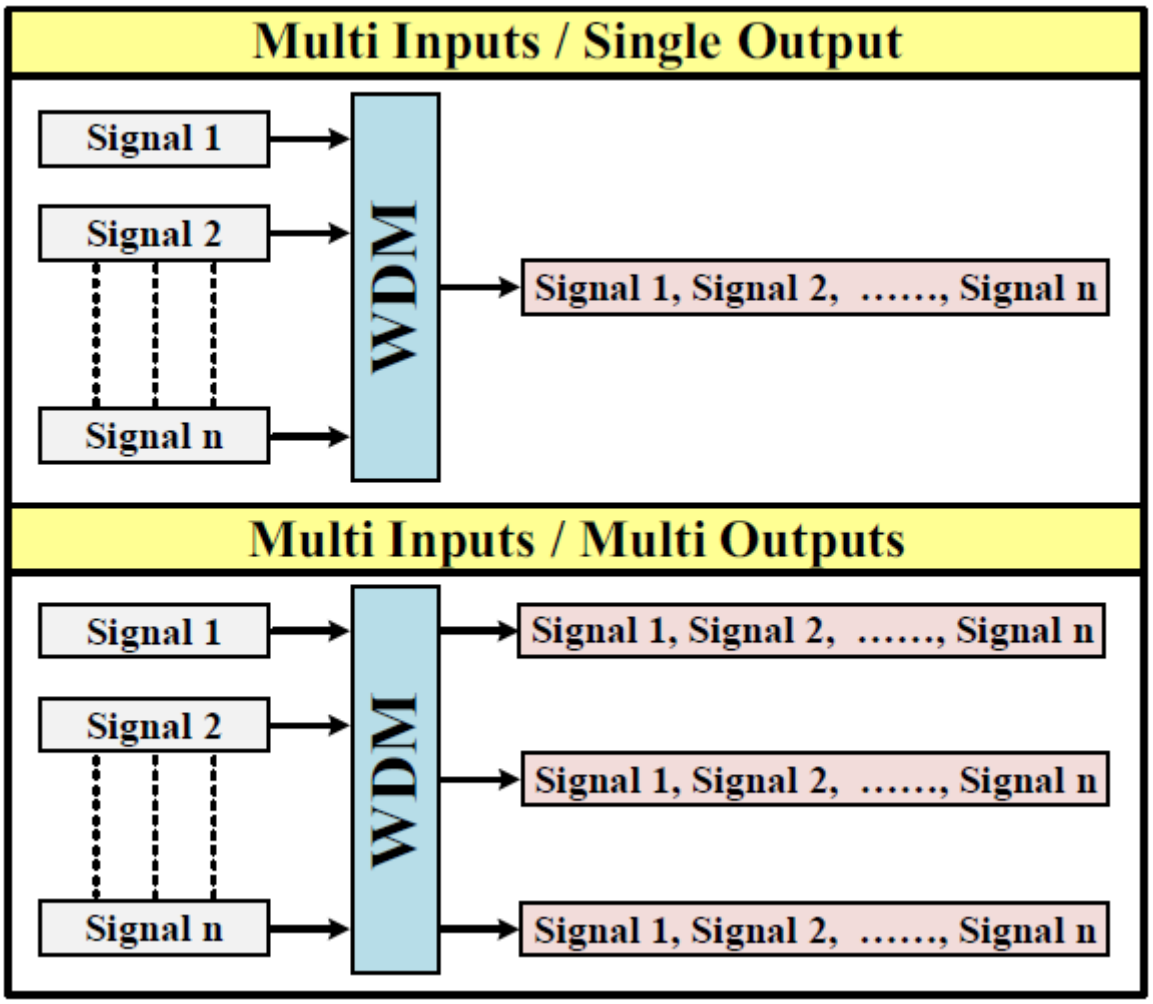

Figure 23

two different algorithms for wavelength division multiplexing technology.

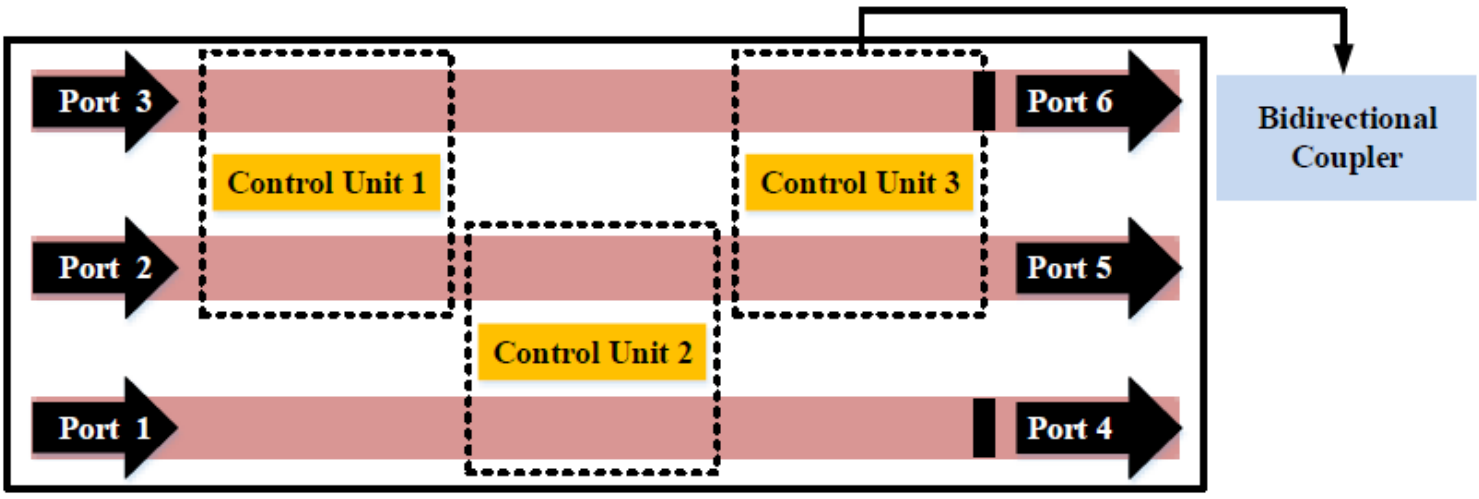

Figure 24

the 2D- XY view of the three-inputs/single-output wavelength division multiplexer.

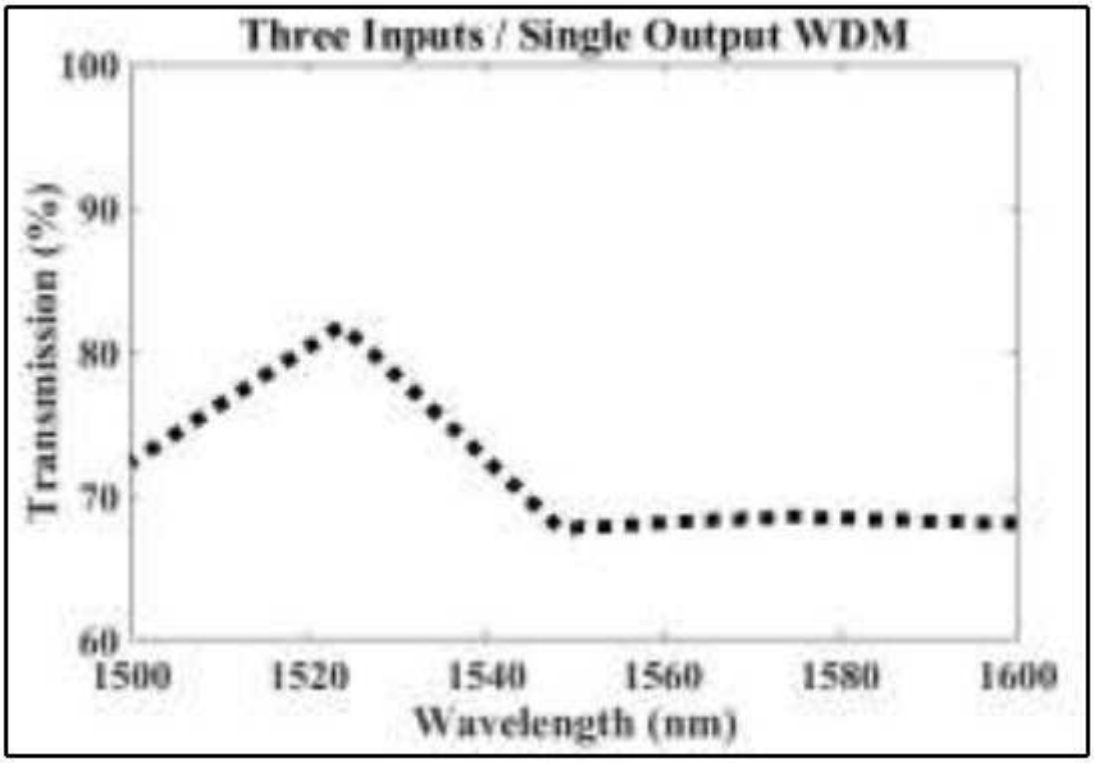

Figure 25

the device' spectrum when input is launched into port (1).

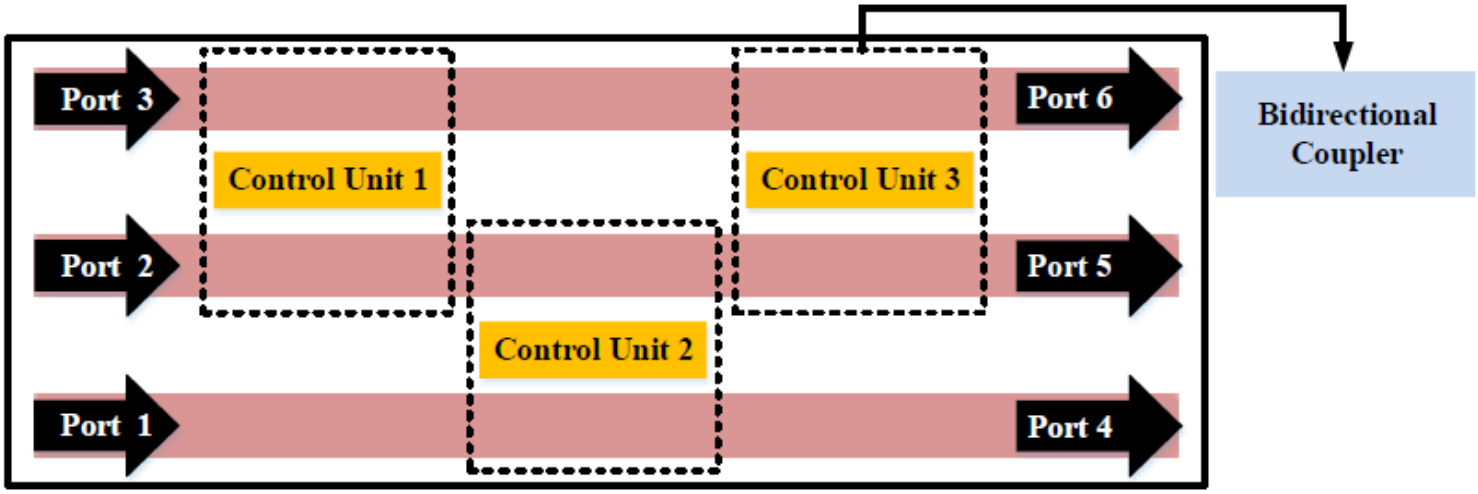

Figure 26

the schematic for three-inputs / three-outputs wavelength division multiplexer.

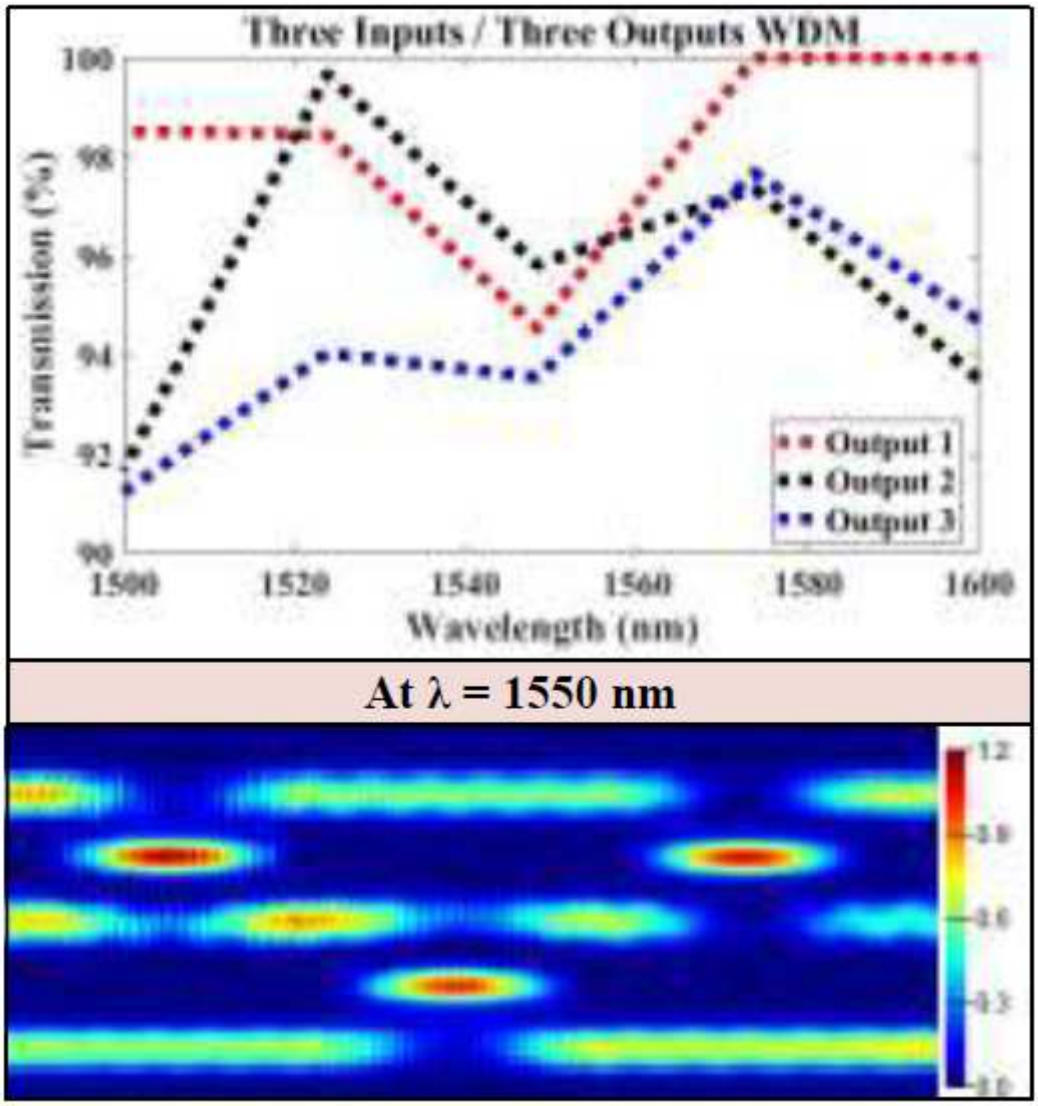

Figure 27

the device' spectrum when input is launched into port (1), and the distribution of electric field (E) intensity for the proposed device.

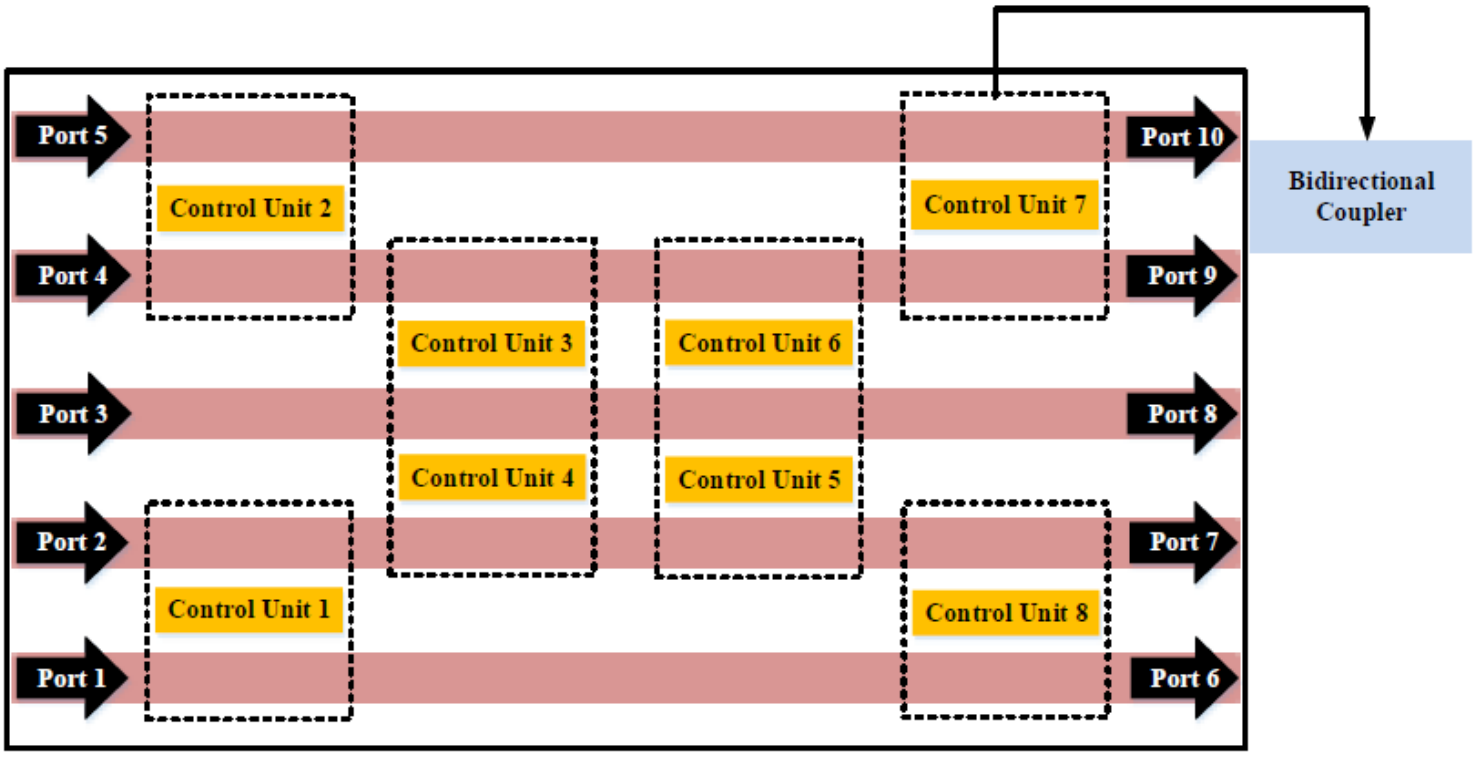

Figure 28

the schematic for hybrid plasmonic 5x5 switching matrix.

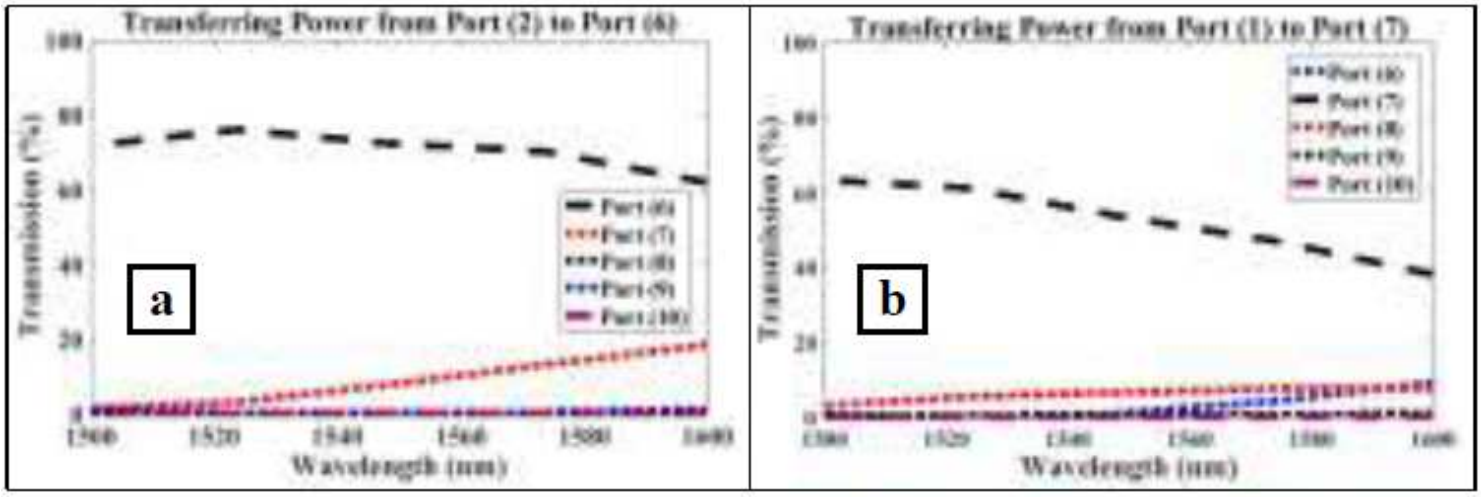

Figure 29

the device' spectrum for a) transferring power from port (2) to port (6), and b) transferring power from port (1) to port (7) as a function of wavelength.

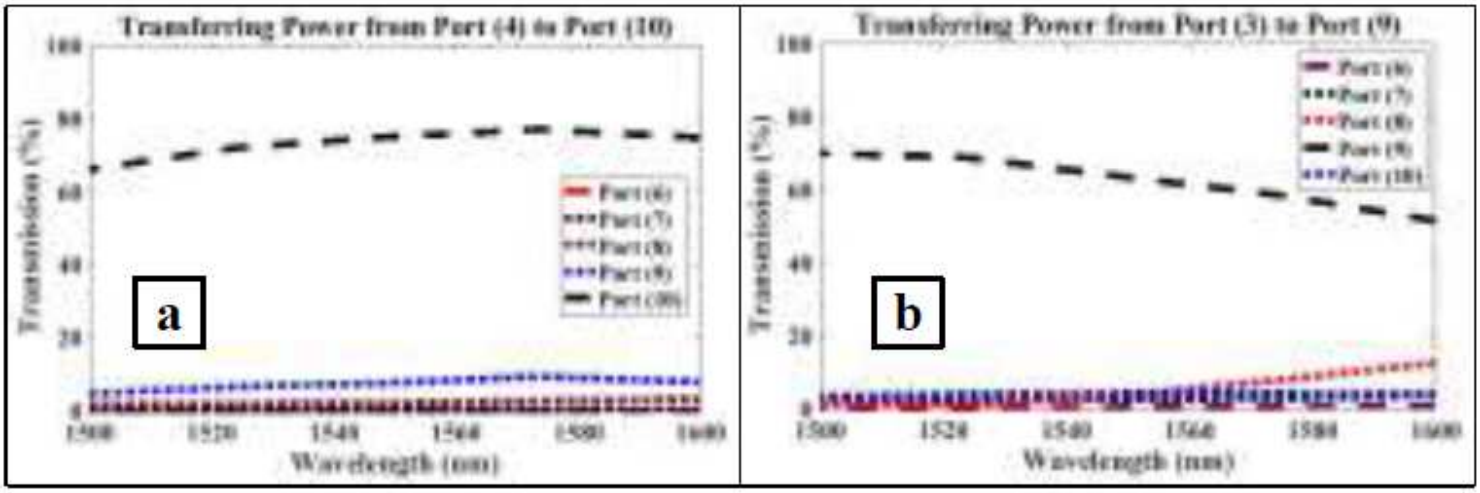

Figure 30

the device' spectrum for a) transferring power from port (4) to port (10), and b) transferring power from port (3) to port (9) as a function of wavelength.

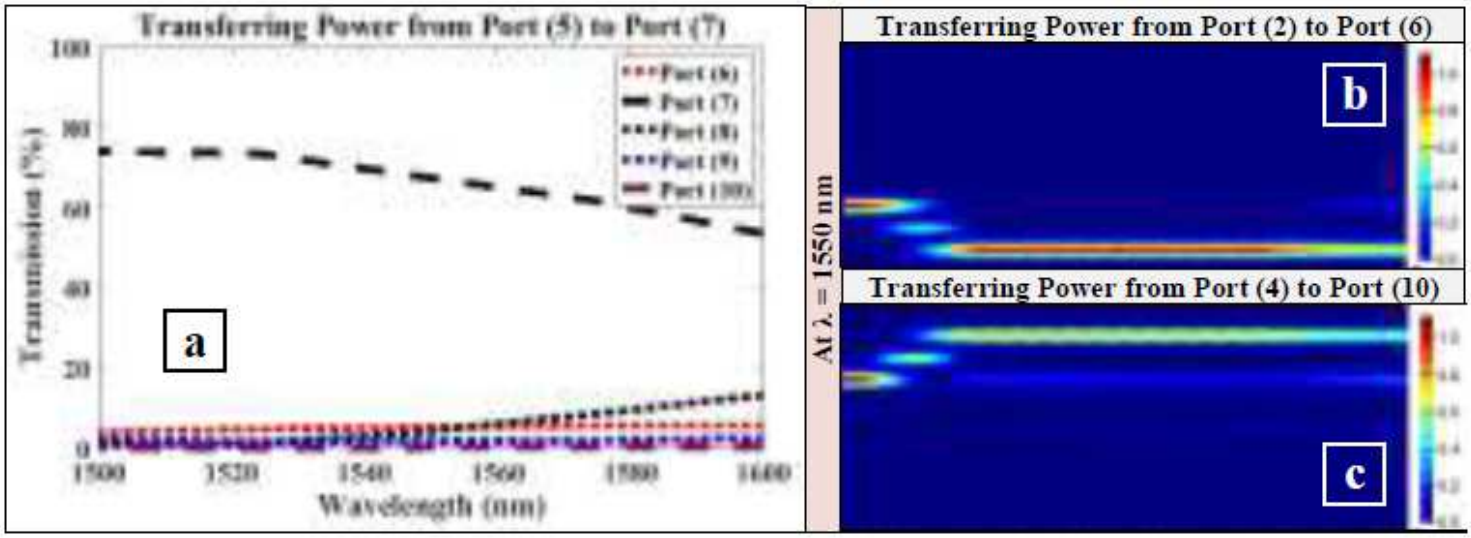

Figure 31

a) the device' spectrum for a) transferring power from port (5) to port (7) as a function of wavelength, b) and c) the field distribution over the device at a wavelength of 1550 nm.

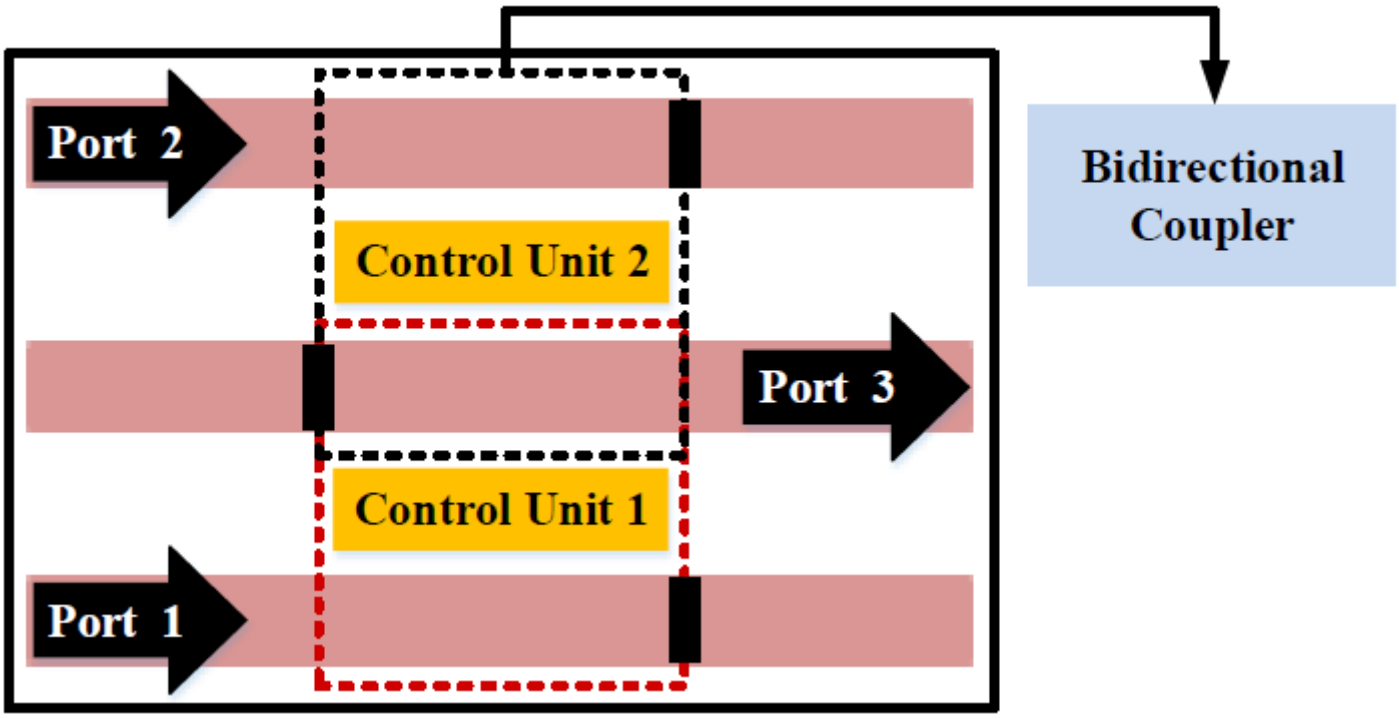

Figure 32

the 2D- XY view of the schematic used for both of the OR and NAND logic gates.

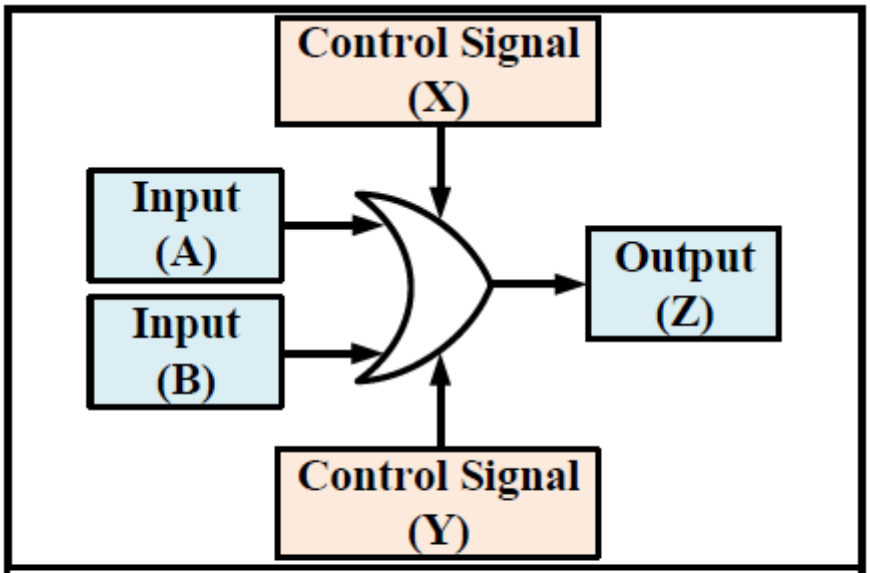

The truth table of OR gate

X	Y	A	B	Z
ON	ON	OFF	OFF	OFF
ON	ON	OFF	ON	ON
ON	ON	ON	OFF	ON
ON	ON	ON	ON	ON

Figure 33

the symbol and the truth table of hybrid plasmonic OR logic gate.

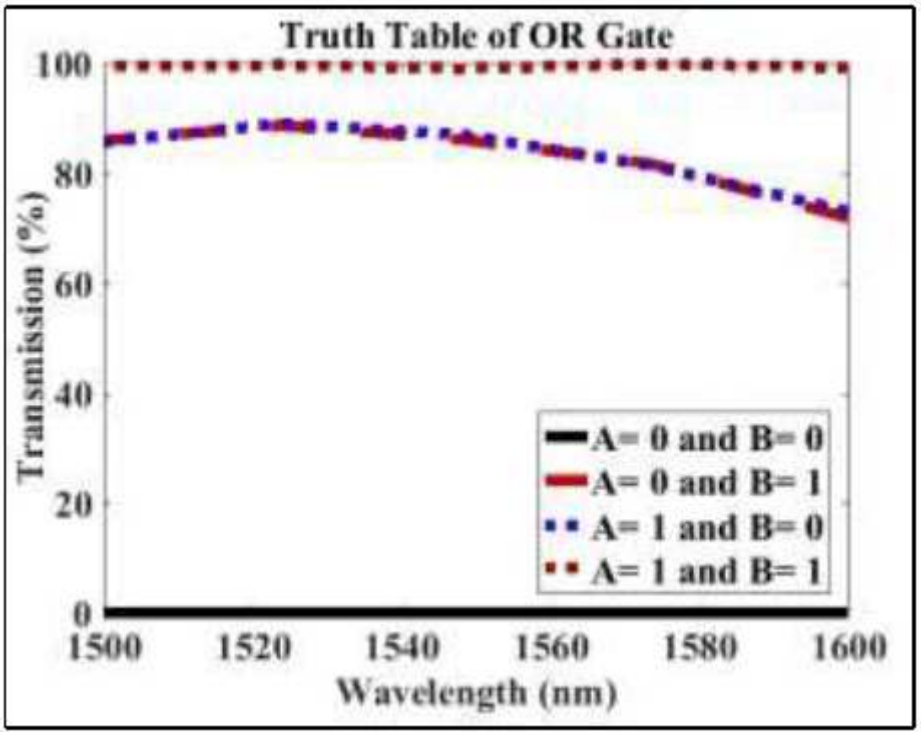

Figure 34

the OR gate performance in terms of transmission as a function of wavelength.

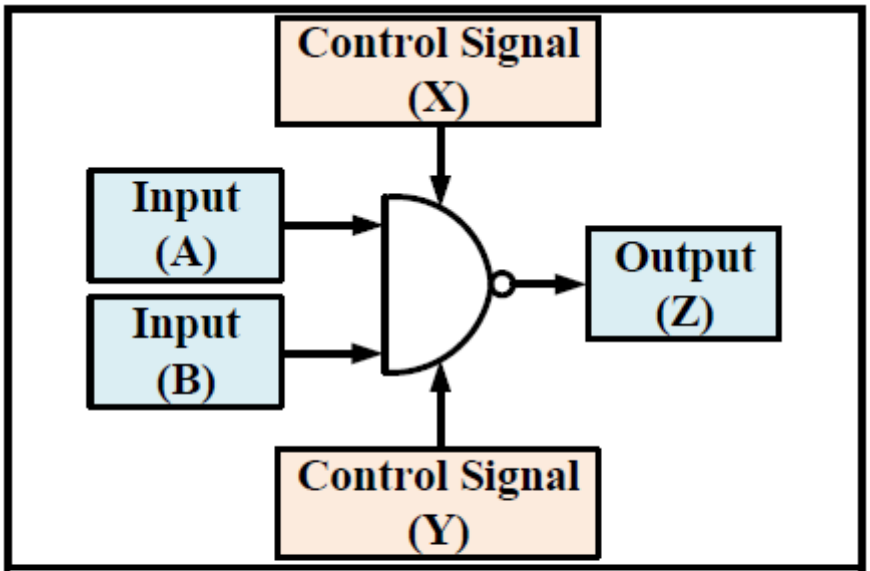

The truth table of NAND gate

A	B	X	Y	Z
ON	ON	OFF	OFF	ON
ON	ON	OFF	ON	ON
ON	ON	ON	OFF	ON
ON	ON	ON	ON	OFF

Figure 35

the symbol and the truth table of hybrid plasmonic NAND logic gate.

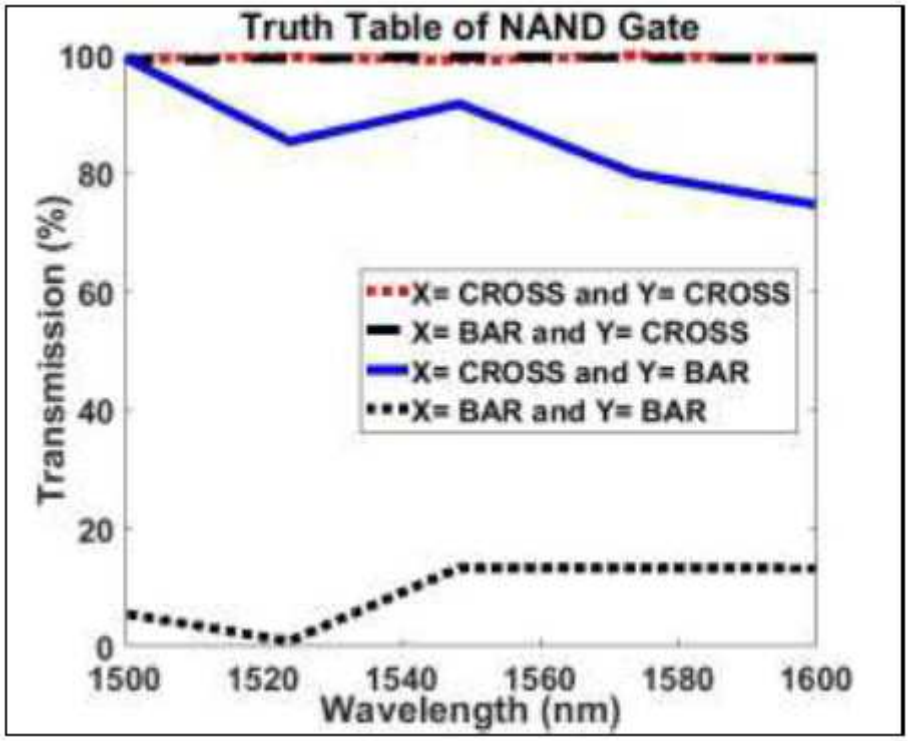

Figure 36

the NADN gate performance in terms of transmission as a function of wavelength.